

# Magnetic Flux of Progenitor Stars Sets Gamma-ray Burst Luminosity and Variability

Alexander Tchekhovskoy<sup>1,2\*</sup> and Dimitrios Giannios<sup>3</sup>

<sup>1</sup>Department of Physics and Department of Astronomy, University of California, Berkeley, CA 94720-3411†

<sup>2</sup>Lawrence Berkeley National Laboratory, 1 Cyclotron Rd, Berkeley, CA 94720, USA

<sup>3</sup>Department of Physics and Astronomy, Purdue University, 525 Northwestern Avenue, West Lafayette, IN 47907, USA

Accepted . Received ; in original form

## ABSTRACT

Long-duration gamma-ray bursts (GRBs) are thought to come from the core-collapse of Wolf-Rayet stars. Whereas their stellar masses  $M_*$  have a rather narrow distribution, the population of GRBs is very diverse, with gamma-ray luminosities  $L_\gamma$  spanning several orders of magnitude. This suggests the existence of a “hidden” stellar variable whose burst-to-burst variation leads to a spread in  $L_\gamma$ . Whatever this hidden variable is, its variation should not noticeably affect the shape of GRB lightcurves, which display a constant luminosity (in a time-average sense) followed by a sharp drop at the end of the burst seen with *Swift*/XRT. We argue that such a hidden variable is progenitor star’s large-scale magnetic flux. Shortly after the core collapse, most of stellar magnetic flux accumulates near the black hole (BH) and remains there. The flux extracts BH rotational energy and powers jets of roughly a constant luminosity,  $L_j$ . However, once BH mass accretion rate  $\dot{M}$  falls below  $\sim L_j/c^2$ , the flux becomes dynamically important and diffuses outwards, with the jet luminosity set by the rapidly declining mass accretion rate,  $L_j \sim \dot{M}c^2$ . This provides a potential explanation for the sharp end of GRBs and the universal shape of their lightcurves. During the GRB, gas infall translates spatial variation of stellar magnetic flux into temporal variation of  $L_j$ . We make use of the deviations from constancy in  $L_j$  to perform stellar magnetic flux “tomography”. Using this method, we infer the presence of magnetised tori in the outer layers of progenitor stars for GRB 920513 and GRB 940210.

**Key words:** MHD — gamma-rays: stars — methods: numerical — methods: analytical — stars: magnetic field

## 1 INTRODUCTION

Long-duration GRBs are believed to be associated with the collapse of the core of massive stars. This association is very firm in GRBs accompanied by supernovae explosions (Stanek et al. 2003; Galama et al. 1998). The nature of the supernova (type Ic) indicates Wolf Rayet stars of spectral type WO/C as the progenitors. Such stars have mass  $\sim 10M_\odot$  and radius of  $R \sim$  a few  $R_\odot$ . Despite their masses have a rather narrow distribution, the GRBs they produce come in a very broad range of power. Their luminosity function extends over at least 4 orders of magnitude in  $L_\gamma$  (Wanderman & Piran 2010), and various additional categories of GRBs have emerged in recent years (e.g., Levan et al. 2014).

The observed duration of the prompt emission episode ( $\sim 1 - 100$  sec) roughly agrees with the free-fall time scale of the progenitor star. The GRB emission is notoriously variable; composed of a large number of intense gamma-ray pulses. Despite

their erratic behaviour, GRBs have some well-defined properties which tightly constrain the models for the central engine. The time-averaged properties of the prompt emission do not evolve in a systematic way with time since the trigger (Ramirez-Ruiz & Fenimore 2000). By looking at a random segment of the GRB lightcurve there is no way to tell from the amplitude and duration of the pulses and the intervals between the pulses whether the segment corresponds to the first or second half of the GRB (Ramirez-Ruiz & Fenimore 2000; Quilligan et al. 2002). This is also demonstrated by the constant slope  $S$  of cumulative counts during GRBs revealing that  $\int_0^t L_\gamma dt \sim \text{constant} \times t$  or  $L_\gamma \sim \text{constant}$  (McBreen et al. 2002). In contrast, the end of the GRB is typically well-defined and is marked by a steep decline in flux. This end stage is seen in X-rays with *XRT* on *Swift*, and is characterised by a steep time-dependence of luminosity, with the flux dropping by several orders of magnitude. This abrupt drop is consistent with an abrupt turn-off of the central engine (see Nousek et al. 2006; Zhang et al. 2006).

This GRB behaviour is hard to understand in the context of core-collapse models irrespective of whether GRBs are powered by accretion onto a black hole (BH, Woosley 1993) or by the rotation

\* E-mail: atchekho@berkeley.edu (AT), dgiannio@purdue.edu (DG)

† Einstein Fellow

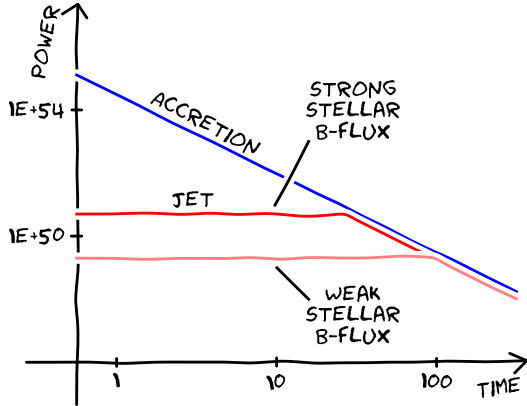


**Figure 1.** A cartoon depiction of accretion and jet power time-dependence during a core collapse. The indicated values along the axes are approximate and intended to give a rough idea of characteristic energy and time scales. At an early time,  $t \lesssim$  few seconds, mass accretion rate is extremely high,  $\dot{M}c^2 \sim M_{\odot}c^2 \text{ s}^{-1} \sim 10^{54} \text{ erg s}^{-1}$ . Soon after core collapse, infalling gas drags into the BH most of progenitor star’s large-scale magnetic flux,  $\Phi_*$ . This flux sets BH jet power,  $L_j \sim 10^{50} \text{ erg s}^{-1} \propto \Phi_*^2$ , which remains approximately constant and *independent of*  $\dot{M}$ . That  $L_j \ll \dot{M}c^2$  means that BH magnetic flux is dynamically subdominant and easily held on the BH by the pressure of the accretion flow. However,  $L_j$  cannot maintain its constancy indefinitely: if jet power remained constant, it would eventually exceed accretion power! But this is impossible: if  $L_j$  substantially exceeds  $\dot{M}c^2$ , BH magnetic flux becomes dynamically-important and cannot be held on the BH by accretion (Tchekhovskoy et al. 2011). As a result, BH magnetic flux diffuses outward, such that jet luminosity tracks the rapidly decaying accretion power,  $L_j \simeq \dot{M}c^2$ . This steep decay of jet luminosity marks the end of the GRB. The stronger the stellar magnetic flux, the more luminous is the GRB: dark and light red lines illustrate the cases of stronger and weaker stellar magnetic fluxes, respectively.

of a neutron star (Usov 1992). How can the average luminosity of the jet, for a minute or so, ignore central engine evolution when the latter is expected to evolve substantially on a similar timescale? What marks the sudden decline in the GRB emission? What sets the GRB luminosity and what causes it to differ so much from burst to burst?

In the magnetar model of GRBs the jet luminosity can be constant for  $\sim 1$  min (set by the spin-down timescale of the magnetar). However, it is unclear what causes GRBs to abruptly end. Moreover, jet properties (baryon loading) evolve fast with time while the average observed GRB spectra do not (see Metzger et al. 2011 for a related discussion).

If the central compact object is a BH, accretion can power GRBs either through neutrino annihilation (Popham et al. 1999; Ruffert & Janka 1999; Birkel et al. 2007; Chen & Beloborodov 2007; Zalamea & Beloborodov 2011) or magnetic energy extraction (Narayan, Paczyński & Piran 1992; Levinson & Eichler 2003; Meszaros & Rees 1997). After the core collapse, the accretion rate  $\dot{M}$  drops fast with time unless one makes very particular choices for the progenitor star and the accretion disk viscosity (Kumar et al. 2008a,b). In any jet production mechanism, which depends on the instantaneous BH mass accretion rate,  $\dot{M}$ , the observed constancy of the GRB luminosity requires fine tuning: in order to obtain an approximately constant jet luminosity, the efficiency of jet production must increase with time in exactly the right way so as to precisely cancel the effect of decrease in  $\dot{M}$ .

This monotonic decrease of  $\dot{M}$  with time challenges neutrino models where the jet power scales with accretion rate as  $L_j \propto \dot{M}^{9/4}$  (or a similar steep power; see Zalamea & Beloborodov 2011). Even a weak systematic change of the average  $\dot{M}$  throughout the GRB should be easily detectable, which is not the case in the majority of the bursts. The mechanism also cannot account for the energetics of the longest bursts observed (Leng & Giannios 2014).

Here we argue that it is the *magnetic flux through the collapsing star that determines the luminosity of the jet*, as we illustrate in Fig. 1. Indeed, if the jet is launched via magnetic fields, the accretion rate does not always determine the jet power directly (Tchekhovskoy, Narayan & McKinney 2011; see however Krolik & Piran 2011). The available magnetic flux in the progenitor star may be much more constraining (Komissarov & Barkov 2009). The flux accumulates on the newly formed BH on a timescale shorter than the time it takes for the jet to emerge from, or break through, the collapsing star.

We assume that the jet is powered by the large-scale magnetic flux via the Blandford-Znajek process (BZ, Blandford & Znajek 1977). In this picture, as in most collapsar models, the jet breakout marks the start of the prompt emission, or the GRB trigger. From then on and until the end of the GRB, for reasonable collapsar parameters, the mass of the BH  $M_{\text{BH}}$ , the magnetic flux through the hole  $\Phi_{\text{BH}}$ , and BH spin  $a$  evolve little over the GRB duration. So long as the mass accretion rate  $\dot{M}$  is sufficiently high to sustain the magnetic flux  $\Phi_{\text{BH}}$  on the BH, jet luminosity  $L_j \propto a^2 \Phi_{\text{BH}}^2 M_{\text{BH}}^{-2}$  is *independent of*  $\dot{M}$  and is approximately constant, as illustrated in Fig. 1 with horizontal segments of red lines. However, since  $\dot{M}$  asymptotically approaches zero, eventually  $\dot{M}$  becomes too low to confine the magnetic flux of a constant strength on the BH. This occurs at the equipartition between accretion and jet powers,  $\dot{M}c^2 \simeq L_j \sim 10^{50} \text{ erg s}^{-1}$ , or, in terms of mass accretion rate,  $\dot{M} \sim 10^{-4} M_{\odot} \text{ s}^{-1}$ . From this point on the accretion disk cannot hold the entirety of magnetic field on the BH anymore. The remaining flux on the BH stays in equipartition with accretion power, and the jet luminosity scales linearly with  $\dot{M}$ , which rapidly declines toward zero and causes the GRB to end abruptly.

We start with the description of progenitor star’s structure and its core-collapse in Sec. 2, paying particular attention to how the central BH properties – mass, spin, and magnetic flux – change in time. In Sec. 3 we derive the time-evolution of jet power and in Sec. 4 perform the comparison of our model to the observed GRB light curves. In Sec. 5 we conclude. Throughout the paper, we use Gaussian-cgs units.

## 2 COLLAPSAR MODELS

We consider GRB jets that are powered by the accretion onto the central BH. To compute the rate at which the BHs are fed with gas, we consider several pre-collapse stellar models described in Woosley & Heger (2006). We focus in this section on the “16TT” model of a pre-collapse star at 1% solar metallicity. The model includes a treatment of magnetic dynamo effects and mass and angular momentum loss via stellar winds. Figure 2(a) shows the density profile in the pre-collapse star: outside the core,  $R \gtrsim 10^8 \text{ cm}$ , the density falls off roughly as a power-law,  $\rho \propto r^{-2.5}$ , and cuts off exponentially toward the surface, at  $r_* \simeq 5 \times 10^{10} \text{ cm}$ . Figure 2(b) shows the radial distribution of angular momentum. It has clear discontinuities, which result from transitions between different shells of stellar structure. To get a sense of the variety in GRB progenitors, we also consider two other progenitor models, 16TH

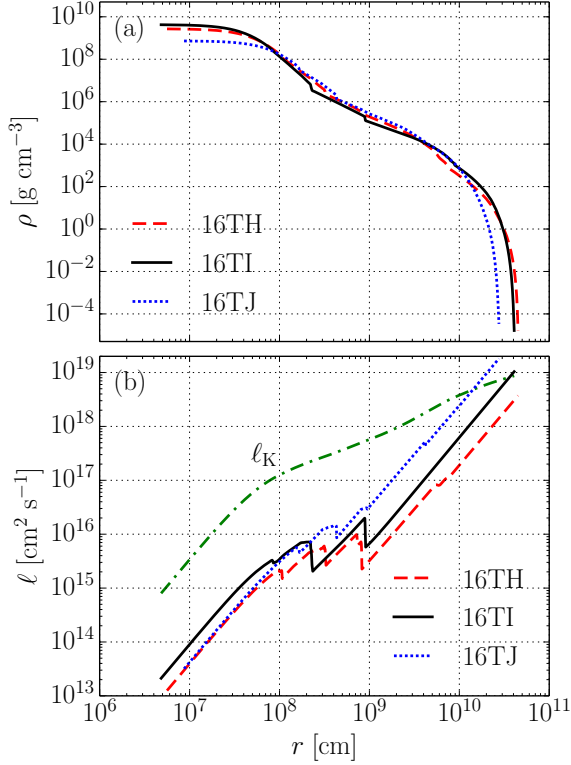


**Figure 2.** Structure of GRB stellar progenitor models (Woosley & Heger 2006), 16TH, 16TI, and 16TJ, which are shown with red dashed, black solid, and blue dotted lines (see legend). **[Panel a]:** Radial profile of stellar density,  $\rho$ . Density is approximately constant inside the stellar core,  $r \lesssim 10^8$  cm, and falls off approximately as a power-law in radius outside of the core,  $\rho \propto r^{-2.5}$ , until the surface of the star,  $r_* \sim \text{few} \times 10^{10}$  cm, where it exponentially drops. **[Panel b]:** Radial profile of specific angular momentum for the three models, which are shown with the same colours as in panel (a). For comparison, we also show the Keplerian angular momentum,  $\ell_K$ , with green dash-dotted line. Discontinuities in the radial distribution reflect shells in stellar structure. Near the surface of the star, the angular momentum exceeds the Keplerian value.<sup>1</sup>

and 16TJ, which differ from the fiducial model by the strength of stellar winds, and we show them in Fig. 2 for comparison. As we will see below, our main conclusions do not depend on the details of model (see Section 3.5).<sup>1</sup>

<sup>1</sup> Note that stellar rotation profile is uncertain due to the limitations of the 1D stellar models and uncertainties in the treatment of microphysics of turbulence, magnetic fields, and stellar winds. For instance, the angular momentum  $\ell = (2/3)\Omega r^2$ , in models 16TH and 16TJ exceeds the Keplerian value,  $\ell_K$ , in the outer layers of the star (see Fig. 2b). If the outer layers indeed were super-Keplerian, the star would have already expelled these outer layers long before core collapse. These extremely high values appear due to the uncertainties of angular momentum transport inside the outer layers of the star and angular momentum extraction by the stellar winds and are not physical (Woosley & Heger 2006). For this reason, for our calculations, we modify the rotational profile of the models and limit the angular momentum to be at most 10% of the local Keplerian value (see Fig. A1(a) for an example; our results are not sensitive to the particular value of the cutoff). Apart from this modification, we adopt the rotational profile of the models as is, to illustrate the robustness of our results.

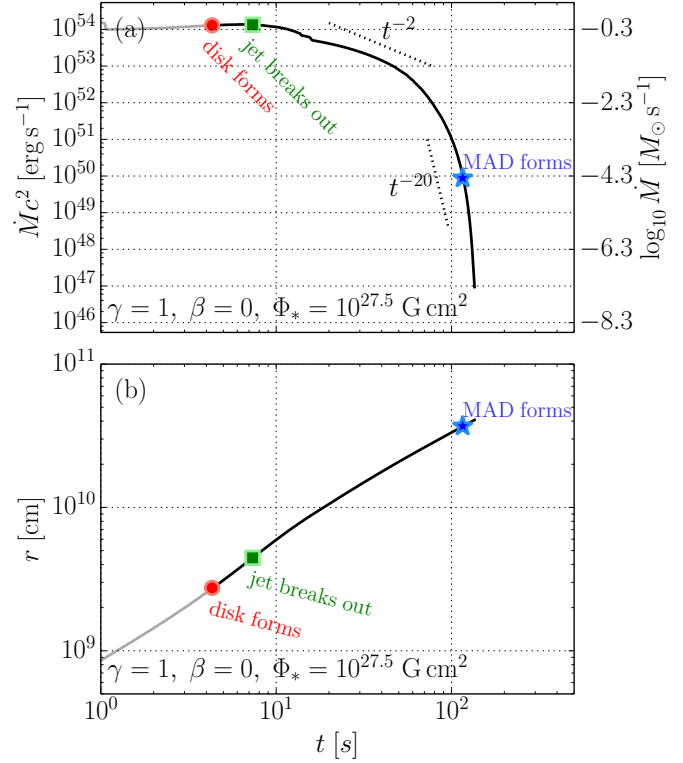


**Figure 3.** **[Panel (a):** Mass accretion rate  $\dot{M}$  vs. time since core collapse  $t$  for our fiducial pre-collapse stellar progenitor model, 16TI (Woosley & Heger 2006). For the sake of later discussion, the time of disk formation is indicated with a red circle, jet breakout with the green square, and emergence of a dynamically-important magnetic field threading the BH (or the magnetically-arrested disk, MAD), with the blue star, at which the GRB ends (see Sec. 2.2). The latter two of these times depend on progenitor star's magnetic flux strength (described by  $\Phi_*$ ) and radial distribution (described by  $\gamma$ , see eq. 8), and the mass-loss from an accretion disk (described by  $\beta$  see eq. 11). **[Panel (b):** The mapping between the the radial position  $r$  of a layer of gas in the progenitor star and the time  $t$  since core collapse at which it reaches the BH.

## 2.1 Temporal evolution of the GRB central engine

The collapse of the core causes the star to lose pressure support, and the star evolves on the free-fall timescale  $t_{\text{ff}} \equiv r_*/v_{\text{ff}} = (r_*^3/2GM_*)^{1/2} \sim 130$  s. We assume that shortly after the core collapses, a BH forms. The density profile of the star determines the growth rate of the BH. The rotational profile of the collapsing star, shown in Fig. 2(b), controls which layers of the star collapse directly into the BH. The total angular momentum  $J(t)$  and mass  $M(t)$  of the layers that collapsed determine the evolution of BH spin  $a = J/Mr_g c$ . When the specific angular momentum of a layer exceeds that of a test particle orbiting at the innermost stable circular orbit (ISCO),  $l_{\text{ISCO}}$ , the fallback accretion hits the centrifugal barrier, circularises and forms an accretion disk. When a disk is present, the specific angular momentum of the material that ac-

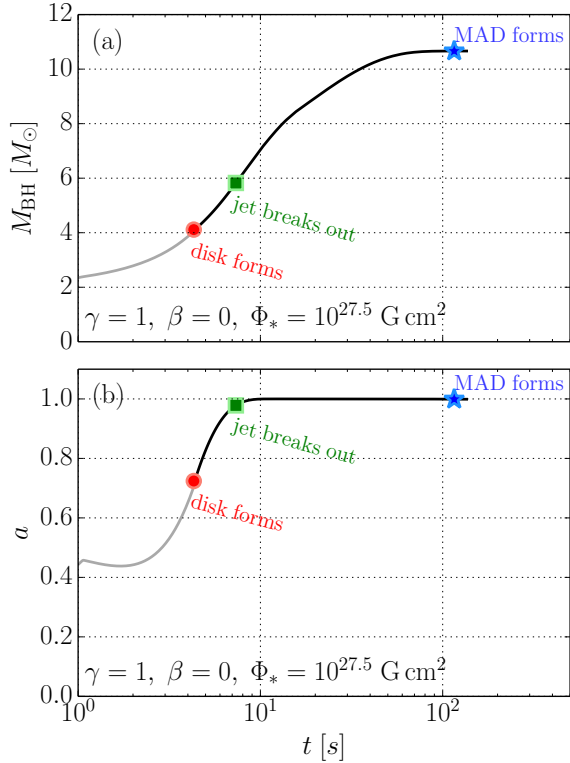


**Figure 4.** Black hole mass  $M_{\text{BH}}$  (panel a) and spin  $a$  (panel b) vs. time  $t$  since the core-collapse for our fiducial model. Red circle indicates the time of accretion disk formation and green circle indicates the time of the jet breakout, which we associate with the gamma-ray trigger. Blue stars mark the time at which the magnetic flux on the BH becomes dynamically-important, a magnetically-arrested disk (MAD) forms, and the GRB ends. See Fig. 3 for details.

cretos on the black hole is set equal to  $t_{\text{ISCO}}^2$ . We now discuss these processes in more detail.

In Fig. 3(a) we show mass inflow rate  $\dot{M} \equiv 4\pi R^2 \rho(R) v_{\text{ff}} = 4\pi R^3 \rho(R) / t_{\text{ff}}$  as a function of time since core collapse. For our fiducial model, the formation of the disk takes place at  $t_{\text{disk}} \approx 4$  seconds post core collapse and is indicated in Fig. 3(a) with red circles. As seen in Fig. 3(b), at this early time the BH accretes dense, inner layers of the star,  $r \sim \text{few} \times 10^9$  cm, and the mass accretion rate is very high  $\dot{M} \sim M_{\odot} \text{ s}^{-1}$ .<sup>3</sup> The accretion power,  $\dot{M} c^2 \sim 10^{54}$  erg  $\text{s}^{-1}$ , by many orders of magnitude exceeds the upper range of GRB luminosity,  $L_j \sim 10^{50}$  erg  $\text{s}^{-1}$ . This implies that, at least at early times, magnetic fields are dynamically subdominant relative to the accretion flow (we discuss this in Sec. 2.2.2).

We assume that the formation of the centrifugal barrier and of

<sup>2</sup> We assume that the timescale for the material to reach the BH is dominated by the free-fall time  $t_{\text{ff}}$  and not by the accretion time  $t_{\text{acc}}$ . We have checked that for judicial viscosity parameter  $\alpha = 0.1$ , and disk aspect ratio  $H/R \sim 1$ , the accretion timescale is nearly always shorter than the free-fall time of the star. In this paper, for simplicity and transparency, we ignore the modifications to the time it takes the gas to reach the BH due to the formation of an accretion disk (see Appendix A).

<sup>3</sup> Here we equate the inflow rate of mass from the collapsing star to the accretion rate to the black hole. In effect, we ignore mass loss that can take place though, e.g., winds from an accretion disk. Wind mass loss is considered in Sect. 3.3.

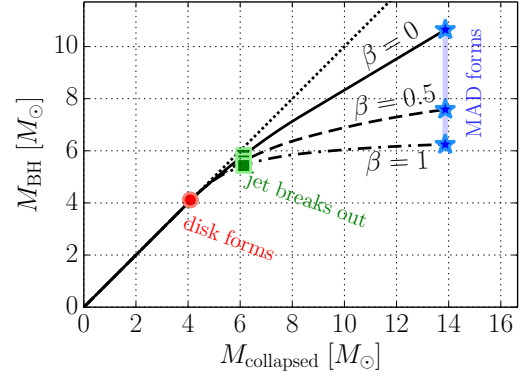


**Figure 5.** Dependence of BH mass on the collapsed stellar mass for our fiducial stellar model 16TI (Woosley & Heger 2006). The solid line shows the mass of the BH for our fiducial model, which does not include any mass-loss from the accretion disk ( $\beta = 0$ , see eq. 11). The dotted line shows the line of equal masses. The final  $M_{\text{BH}}$  is lower than  $M_{\text{collapsed}}$  by about 30%. This is due to the fact that during accretion on a rapidly spinning BH, a substantial part of the mass-energy is carried away by neutrinos, disk winds, etc. Dashed and dash-dotted lines show cases with mass loss from the accretion disk:  $\beta = 0.5$  and 1, respectively (see eq. 11 for  $\beta$  definition). The presence of mass-loss further decreases the mass of the BH. The time of disk formation is indicated with the red circle, jet breakout with green square, and MAD formation with blue stars (which are connected with a solid light blue).

the disk opens up a low-density polar funnel region through which the jet emerges. The jet is powered by BH rotation and large-scale magnetic fields threading the BH (see Section 3 for a discussion of jet properties). The jet takes several seconds to drill a hole through the collapsing star. The GRB trigger takes place at the moment the jet emerges, or “breaks out”, of the star. For our fiducial model this happens a few seconds after disk formation, at  $t \approx 7$  seconds after core-collapse, as indicated with green squares in Fig. 3. The trigger occurs early in time,  $\lesssim 10$  s after the core collapse, while mass accretion rate is still very high. We adopt the following expression for jet breakout time (Bromberg et al. 2014a,b):

$$t_{\text{breakout}} - t_{\text{disk}} = \left( \frac{L_j}{2 \times 10^{50} \text{ erg s}^{-1}} \right)^{-1/3} \left( \frac{M_*}{15 M_{\odot}} \right)^{1/3} \left( \frac{r_{\text{H}}/a}{1.25 \times 10^6 \text{ [cm]}} \right)^{2/3} \text{ [s]}, \quad (1)$$

which is the difference between the time it takes the jet head to traverse the star and the light travel time across the star. Here  $r_{\text{H}} = r_{\text{g}}[1 + (1 - a^2)^{1/2}]$  is the radius of BH event horizon,  $L_j$  is jet power (of both jets) at disk formation, and  $M_*$  the progenitor mass. Estimate (1) accounts for the fact that deep inside the star the velocity of jet’s head is non-relativistic: whereas the most powerful jets take roughly a light crossing time to drill through the star and break out of it (and therefore  $t_{\text{breakout}} - t_{\text{disk}} \approx 0$ ), weaker jets or jets powered by slowly rotating BHs propagate slower and take a longer time. As we will see below, qualitatively, our results are insensitive to the particular expression for jet breakout time.

Figure 4 shows how BH mass and spin change during the core collapse: after the GRB trigger, BH mass changes by no more than a factor of 2 and the spin is practically unchanged,  $a \approx 1$ . Due to the high value of BH spin, the gas that reaches the BH from the ISCO is strongly gravitationally bound to the BH. The strong binding can be achieved because a substantial fraction of rest-mass energy is lost in the form of neutrinos, disk winds, etc. Energy loss

suppresses the rate of BH growth: the black solid line in Fig. 5 shows that the final BH mass is about 30% less than the mass of the collapsed star. In Sec. 3.3 we discuss another potential mechanism that can be operating in accretion flows and that can also lead to the suppression of BH growth: mass loss from the accretion disk.

At late time,  $t \gtrsim 50$  seconds, the BH starts to consume the outer layers of the star (see Fig. 3b), in which the density has a particularly steep radial profile (see Fig. 2a), and the time-dependence of mass accretion rate steepens exponentially, with effective power-law scaling as steep as  $\dot{M} \propto t^{-20}$  (see Fig. 3a). Thus, we see that despite the mass accretion rate rapidly evolving in time, BH mass and spin saturate around the start of the GRB and do not change appreciably after that, with important consequences for jet power that we now discuss.

## 2.2 Available magnetic flux and jet power

An important factor that controls jet power is large-scale magnetic flux threading the BH (i.e., the flux that crosses the BH event horizon). It is conceivable that this flux is dragged to the BH by the collapsing stellar gas. We first argue that the star can contain the necessary magnetic flux to power a GRB and then show that the accretion disk can hold this flux on the BH for a minute or so. We then suggest that this timescale is what sets the GRB duration.

### 2.2.1 Magnetic field strength on the hole

Can the strength of the magnetic flux on the BH be limited by the amount of magnetic flux available in the progenitor star? To find this out, we will assume that a progenitor star, similar to model 16TI of Woosley & Heger (2006), has a magnetic field of  $B_{\text{surf}} \sim 10^4$  G at the surface, which is located at  $r_* \approx 5 \times 10^{10}$  cm. Since GRBs are rare events (Guetta et al. 2005), such a strong surface magnetic field might not be uncommon among GRB progenitors.

Part of the core, with radius  $r_{\text{coll}} \approx 3 \times 10^9$  cm (see Fig. 3b), directly collapses and forms a black hole of mass  $M_{\text{BH}} \approx 4M_{\odot}$  (Fig. 4a) and gravitational radius  $r_g = GM_{\text{BH}}/c^2 \approx 6 \times 10^5$  cm. Assuming dipolar field in the star, the magnetic field strength at  $r = r_{\text{coll}}$  before the collapse is  $B_{\text{coll}} = (r_*/r_{\text{coll}})^3 B_{\text{surf}} \approx 5 \times 10^7$  G. If the magnetic field is frozen into the stellar envelope, the direct collapse leads to the field strength at the BH horizon,  $B_{\text{H}} \approx (r_{\text{coll}}/r_g)^2 B_{\text{core}} \approx 10^{15}$  G, or the magnetic flux through the BH of  $\Phi_{\text{BH}} \sim 5 \times 10^{27}$  G cm<sup>2</sup>. The resulting jet power,

$$L_{\text{BZ}} \approx \frac{kf}{4\pi c} \Phi_{\text{BH}}^2 \Omega_{\text{H}}^2, \quad (2)$$

is  $\sim 10^{50}$  erg s<sup>-1</sup>, where  $k \approx 0.05$  and  $\Omega_{\text{H}} = ac/(2r_{\text{H}})$  is the angular frequency of BH horizon (Tchekhovskoy et al. 2010). We will refer to the expression for BZ power, given by eq. (2) with  $f = 1$ , as the second-order ‘BZ2’ approximation: it is accurate for  $a \lesssim 0.95$ . For our numerical models, which we describe in Sec. 3, we will make use of a more accurate sixth-order ‘BZ6’ expression for jet power that is valid for all values of spin and includes a high-order correction factor,  $f = 1 + 0.35\omega_{\text{H}}^2 - 0.58\omega_{\text{H}}^4$ , where  $\omega_{\text{H}} = a/[1 + (1 - a^2)^{1/2}]$  is the dimensionless rotational frequency of BH event horizon.

Thus, a simple estimate (2) shows that the large-scale magnetic flux contained by a progenitor star is sufficient to account for the power of typical long-duration GRBs, around  $10^{50}$  erg s<sup>-1</sup>. This also implies that GRBs seem to require a strongly magnetised pre-collapse core with  $B \gtrsim 10^7$  G. Given that some white dwarfs are

observed with surface magnetic fields in excess of  $\sim 10^8$  G (Kawka et al. 2007; Külebi et al. 2009) such values may be reasonable.

### 2.2.2 Is Jet Power Limited by Available Stellar Magnetic Flux or Mass Accretion Rate?

In Sec. 2.2.1, we found that based on the observed energetics of GRBs, the central BH is threaded by magnetic field of order  $B_{\text{H}} \sim 10^{15}$  G, or magnetic flux  $\Phi_{\text{BH}} \sim 5 \times 10^{27}$  G cm<sup>2</sup>. We showed that it is conceivable that a progenitor star contains this amount of magnetic flux.

What keeps this magnetic flux on the BH? If the accretion ceased, the magnetic flux would have left the BH due to the no-hair theorem. Thus, it is the presence of an accretion disk via its pressure (ram plus thermal) that keeps the magnetic flux on the BH. Immediately after the core-collapse, the mass accretion rate is so high that the pressure of the disk easily overpowers the outward magnetic pressure. However, as  $\dot{M}$  drops, eventually the disk pressure becomes too weak to hold the entirety of magnetic flux on the BH. This happens at a critical mass accretion rate at which accretion and jet power are comparable (Tchekhovskoy et al. 2011, 2012, 2014, Tchekhovskoy, McKinney and Nemmen, in preparation),

$$\dot{M}_{\text{MAD}} c^2 \approx L_j \left(\frac{a}{1}\right)^{-2} \left(\frac{h/r}{0.2}\right)^{-1}. \quad (3)$$

Here  $h/r = 0.2h_{0.2}$  is half-thickness of the inner regions of the accretion disk (the disk is kept relatively thin by neutrino cooling; Chen & Belorodov 2007). In terms of magnetic flux threading the BH,

$$\dot{M}_{\text{MAD}} = 10^{-4} M_{\odot} \text{ s}^{-1} \left(\frac{\Phi_{\text{BH}}}{5 \times 10^{27} \text{ G cm}^2}\right)^2 \left(\frac{M_{\text{BH}}}{10 M_{\odot}}\right)^{-2} \left(\frac{h/r}{0.2}\right)^{-1} \chi^{-2}, \quad (4)$$

where  $\chi = 1.4(1 - 0.38\omega_{\text{H}}) \sim 1$  is a high-order correction.

Typically, collapsars have  $\dot{M} \gtrsim 0.1 M_{\odot} \text{ s}^{-1} \gg \dot{M}_{\text{MAD}} \sim 10^{-4} M_{\odot} \text{ s}^{-1}$ . Thus, the accretion rate onto a newly formed BH is more than sufficient to confine the magnetic flux within the black hole vicinity. And, as long as  $\dot{M} \geq \dot{M}_{\text{MAD}}$ , BH magnetic flux  $\Phi_{\text{BH}}$  is determined by the available stellar magnetic flux and not by mass accretion rate, even though  $\dot{M}$  drops fast with time (see e.g. Fig. 3). Therefore, after the jet emerges through the stellar surface  $\sim 10$  s post core collapse, it powers a GRB of roughly a constant luminosity (see eq. 2), which is illustrated by horizontal segments of the light curves in Fig. 1.

After a minute or so the situation qualitatively changes:  $\dot{M}$  drops below  $\dot{M}_{\text{MAD}}$ , the magnetic flux on the hole becomes dynamically-important, and parts of the flux, which used to thread the BH, diffuse out. The remaining BH magnetic flux obstructs gas infall and leads to a *magnetically-arrested disk* (MAD, Narayan et al. 2003; Igumenshchev et al. 2003; Tchekhovskoy et al. 2011, see also Bisnovaty-Kogan & Ruzmaikin 1974, 1976). The remaining BH magnetic flux is determined by the instantaneous  $\dot{M}$  via eq. (4),

$$\Phi_{\text{BH,MAD}} = 5 \times 10^{27} \text{ G cm}^2 \left(\frac{\dot{M}}{10^{-4} M_{\odot} \text{ s}^{-1}}\right)^{1/2} \left(\frac{M_{\text{BH}}}{10 M_{\odot}}\right) \left(\frac{h/r}{0.2}\right)^{1/2} \chi, \quad (5)$$

and produces jets of energy efficiency, or dimensionless power, given by eq. (3):

$$\eta_{\text{MAD}} \equiv \frac{L_{j,\text{MAD}}}{\dot{M} c^2} \approx a^2 h_{0.2}, \quad (6)$$

i.e., there is a linear relation of  $\dot{M}$  and jet power  $L_{j,\text{MAD}}$  in the MAD regime. Since  $\dot{M}$  rapidly decreases in time, after the MAD onset

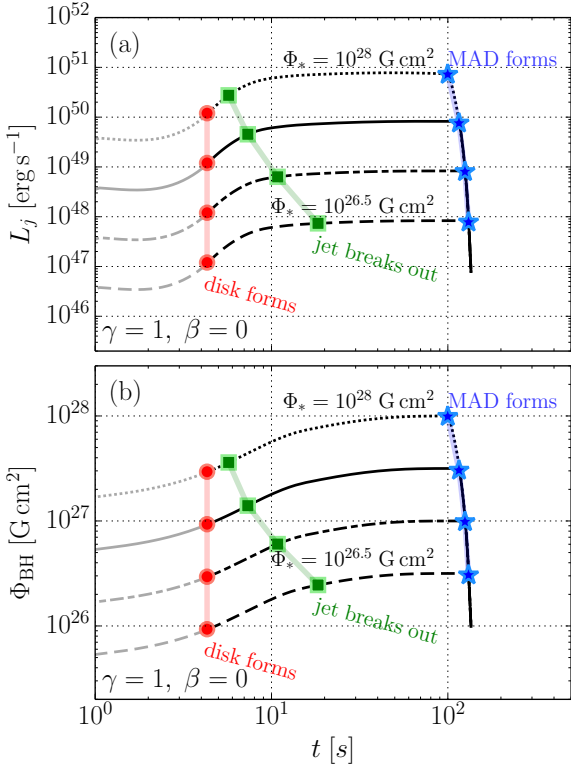


**Figure 6.** Panels (a) and (b) show, respectively, jet power and magnetic flux vs. time, for different values of magnetic fluxes in the progenitor star. Red circles indicate the time of disk formation, green squares jet breakout (=GRB trigger), and blue stars the formation of the MAD (=end of the GRB).

we expect the jet power  $L_{j,\text{MAD}}$  to do so as well. Note that in our numerical models described in Sec. 3, we will use a more accurate expression for jet energy efficiency,

$$\eta_{\text{MAD}} = 3\omega_{\text{H}}^2(1 - 0.38\omega_{\text{H}})^2(1 + 0.35\omega_{\text{H}} - 0.58\omega_{\text{H}}^2)h_{0.2}, \quad (7)$$

which we obtain by combining the high-order accurate versions of eqs. (2) and (5). Equation (6) is a quadratic approximation to the dependence (7).

### 3 EVOLUTION OF JET LUMINOSITY DURING PROMPT PHASE

#### 3.1 Magnetic flux and its distribution in the progenitor

We have argued that GRB jets are powered by the rotational energy of the central BH extracted by large-scale magnetic flux (see eq. 2). Within this framework, in order to get a handle on what determines the luminosity of a GRB, we need to have a better understanding of the processes that control the accumulation of large-scale vertical magnetic flux on the BH.

The growth of the magnetic flux on the BH depends on the very uncertain magnetic field configuration in the progenitor star. However, since the flux is brought in with the accreting gas, it is reasonable to parametrize it to scale with the collapsed mass of the star:

$$\Phi_{\text{BH}}(t) = \Phi_* \left( \frac{M_{\text{collapsed}}}{M_*} \right)^\gamma, \quad (8)$$

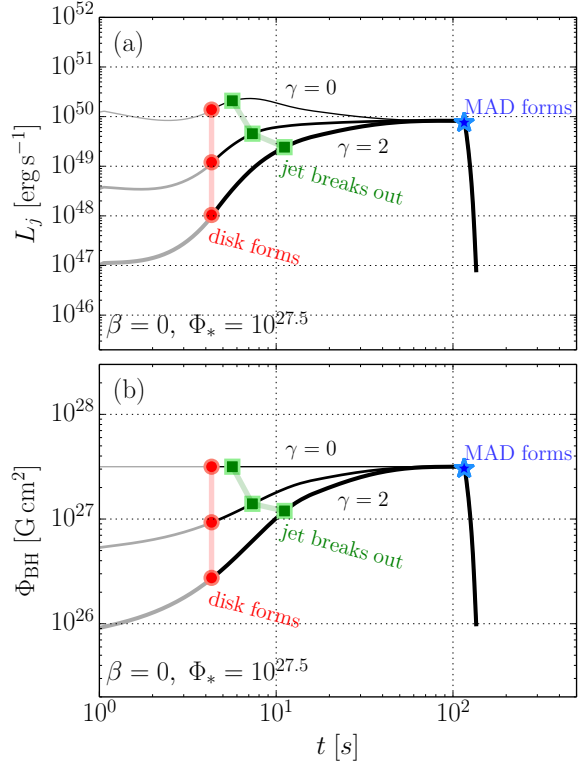


**Figure 7.** Panels (a) and (b) show, respectively, jet power and magnetic flux vs. time, for different distributions of magnetic flux in the progenitor star:  $\gamma = 0$  (thin), 1 (medium-thickness), 2 (thick solid line). Connected red circles show the times of disk formation, green squares the times of jet breakout (=GRB trigger), and blue stars the times of MAD formation (=end of GRB). Variations in spatial distribution of magnetic flux lead to at most variations by factors of a few in GRB luminosity for the different models we considered.

where  $\gamma \sim 1$  parametrizes the radial distribution of magnetic flux inside of the star and  $\Phi_*$  the total magnetic flux threading the star. If we now combine eq. (8) with eq. (2), we obtain:

$$L_{\text{BZ}} \propto \frac{a^2 \Phi_{\text{BH}}^2}{M_{\text{BH}}^2} \propto a^2 M_{\text{BH}}^{2(\gamma-1)}, \quad (9)$$

where we loosely approximated  $M_{\text{BH}} \approx M_{\text{collapsed}}$ . Since BH mass changes by a factor of few in the course of GRB (see Fig. 4a), eq. (9) suggests that the power of the jets changes by the same (small) factor of a few, and this might account for the apparent constancy of GRB prompt emission we set out to explain. We now explore this possibility in detail.

In Fig. 6(a),(b) we plot the time-dependence of jet power, or luminosity  $L_j$ , and the magnetic flux  $\Phi_{\text{BH}}$  threading the BH, for our fiducial scenario,  $\gamma = 1$ . We consider different values of progenitor magnetic flux strength,  $\Phi_* = 10^{26.5}, 10^{27}, 10^{27.5}, 10^{28} \text{ G cm}^2$ , as labeled on the figure and shown with black lines of different types. The behaviour of jet power is very similar, for the entire range of the magnetic flux strength in the progenitor star. After the trigger, which we indicate with the green squares, and until the MAD formation, which we show with blue stars, both magnetic flux and jet power change by about a factor of 2. During this time the strength of magnetic flux on the BH, shown in Fig. 6(b), is determined by the magnetic flux supply in the progenitor star and not by mass accretion rate. Note that for our fiducial model, with  $\gamma = 1$ , by eq. (9) we would expect no dependence of jet power on  $M_{\text{BH}}$  (and time) at

all. As we will see later, there is actually some dependence, caused by the differences between  $M_{\text{BH}}$  and  $M_{\text{collapsed}}$  (see Fig. 5). However, for the entire range we considered,  $0 \leq \gamma \leq 2$ , the variation of  $L_j$  during the GRB is rather weak. After about 100 seconds, a MAD forms, and the luminosity drops fast since the disk cannot hold onto the BH magnetic flux any more and the GRB turns off. We discuss this in detail in Sec. 3.2.

Note that variation by a factor of  $\sim 30$  of the flux  $\Phi_*$  available in the progenitor star, reproduces the full range of observed GRB luminosities ( $L_j \propto \Phi_*^2$ ), from the weakest to the most powerful ones. This range corresponds to surface (core) field strength of the progenitor ranging from  $10^3$  G to  $3 \times 10^4$  G ( $3 \times 10^6 - 10^8$  G). Indeed such a factor of  $\sim 30$  is well within the observed range of variation in the surface field strength of massive stars. The field strength is the only property of the progenitor star that we are aware of, that can plausibly give the large variety of GRB energetics, as observed (see Sec. 3.5).

Figure 7(a),(b) explores the effect of different radial distributions of  $\Phi_*$  in the progenitor star. For this, we plot the time-dependence of  $L_j$  and  $\Phi_{\text{BH}}$  for 3 different values of the  $\gamma$  parameter (defined in eq. 8):  $\gamma = 0, 1, 2$ . The variation in  $\gamma$  affects neither the time of GRB turnoff nor the characteristic power of the GRB, but it does change the early-time trend of jet power dependence on time: for  $\gamma = 0$ , shown with the thin solid line, jet power decreases with time, before levelling off at a constant value. Thus, even though the magnetic flux on the BH is constant in this case (eq. 8), jet power changes: this is because in addition to BH magnetic flux, jet power also depends on the BH mass, whose growth in time leads to the decrease of jet power (see eq. 2). For the other two cases,  $\gamma = 1$  and 2, both  $\Phi_{\text{BH}}$  and  $L_j$  increase with time before levelling off at constant values. We conclude that apart from early time trends, the light curves are not sensitive to the choice of  $\gamma$ .

### 3.2 Steep Decline Phase

Steep decline stage is routinely seen by *Swift*/XRT as a rapid turn-off of GRB luminosity at the end of the GRB, as  $L_j \propto t^{-3..-5}$ . In our model, the steep decline stage starts at the formation of the MAD. In this steep decline stage, we are likely seeing the turn-off of the central engine: the decrease in mass accretion rate below  $\dot{M}_{\text{MAD}}$  (see eq. 4) leads to the MAD state, in which the jet power tracks the rapidly declining  $\dot{M}$ . Thus, we can conclude that the observed steep decline is the natural result of the central BH accreting the outer layers of the star. In fact, we find that the jet power drops extremely steeply,  $L_j \propto \dot{M} \propto t^{-20}$  or so. The resulting gamma-ray luminosity,  $L_\gamma$ , will experience a shallower decline, depending on the size of the emitting region (Kumar & Panaitescu 2000). Thus, in order to explain the observed decline,  $L_\gamma \propto t^{-3..-5}$ , the jet has to turn-off *at least* as steeply as the bursts are observed to decline, which is consistent with our findings.

What sets the duration of the GRB in our model? There are at least two parameters: the strength of the magnetic flux threading the star,  $\Phi_*$ , and the density distribution in the outer layers of the star, which sets the late-time dependence of  $\dot{M}$ . Since the strength of  $\Phi_*$  can be inferred from GRB jet luminosity via eq. (2), the end of the GRB signals the time at which  $\dot{M} = \dot{M}_{\text{MAD}}$  (see eq. 4), i.e., the accretion flow onto the BH enters the MAD regime. Since MADs around rapidly spinning BHs give  $L_j \approx \dot{M}c^2$  (see eq. (3)), we can estimate mass accretion rate at the end of the GRB as

$$\dot{M}_{\text{turnoff}} = \frac{L_j}{c^2} = 0.6 \times 10^{-4} M_\odot \text{ s}^{-1} \frac{L_j}{10^{50} \text{ erg s}^{-1}}. \quad (10)$$

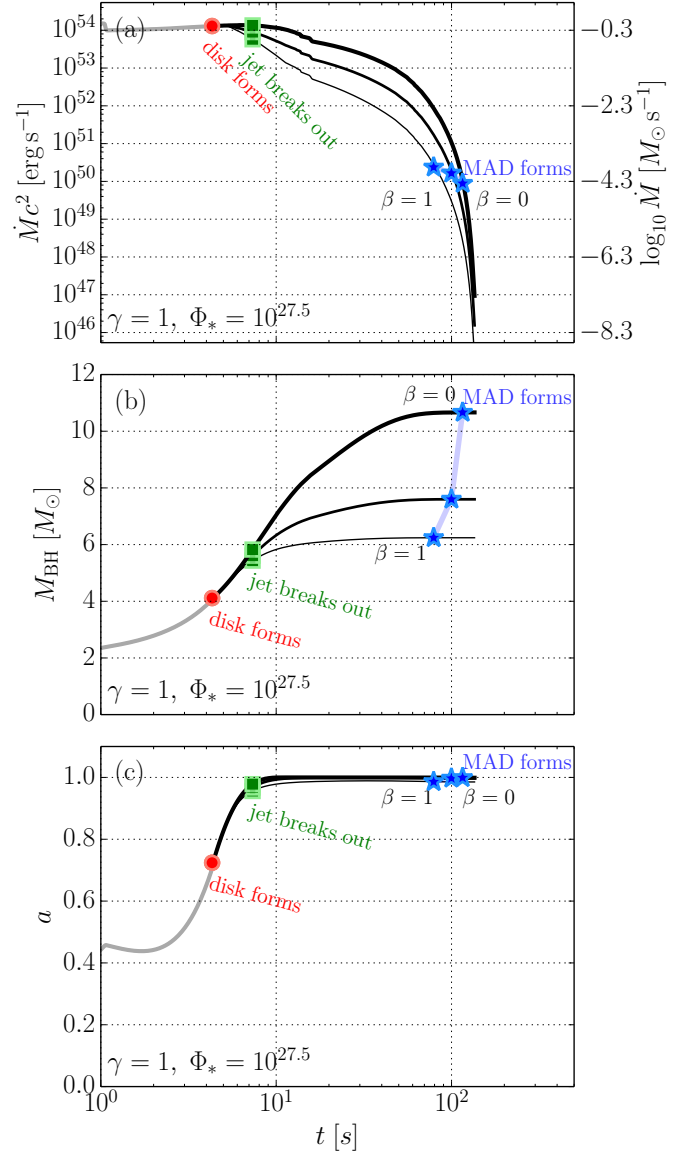


**Figure 8.** Mass accretion rate  $\dot{M}$ , BH mass  $M_{\text{BH}}$ , and BH spin,  $a$  as a function of time for the case when we explore the effect of mass loss in a wind from an accretion disk. The mass-loss is modelled through suppression of  $\dot{M}$  versus radius,  $\dot{M} = (10r_g/r_D)^\beta \dot{M}_D$ , where  $r_D$  is the outer radius of the accretion disk. We explore three different  $\beta$  values: 0, 0.5, and 1.

Since, according to eq. (4), we have  $\dot{M}_{\text{MAD}} \propto \Phi_{\text{BH}}^{1/2}$ , stronger BH magnetic flux translates into a higher mass accretion rate at GRB turn-off. Therefore, for larger  $\Phi_{\text{BH}}$  and all else being equal, we would expect the GRB to be more powerful and last for a shorter time. However, this effect is diluted by the fact that more powerful jets breakout faster and thus we start seeing GRB earlier (see eq. 1). We will also see later (Sec. 3.4) that changes in stellar angular momentum profile strongly affect the jet breakout time and the GRB duration.

### 3.3 Mass loss from the disk

So far we have assumed that all the mass from the collapsing star makes it to the black hole. In reality, stellar material settles into a

disk with an outer size  $r_D$ , which is set by the value of the specific angular momentum  $\ell$  of the stellar material,  $r_D \approx \ell^2/GM$ , where  $M$  is the enclosed mass. For outer layers of the star,  $r_D$  can be much larger than  $r_{\text{ISCO}}$ , and substantial mass loss can take place between the two radii (Blandford & Begelman 1999; McKinney et al. 2012; Narayan et al. 2012; Sądowski et al. 2013, 2014)

We model the effect of mass loss in a standard way, assuming that winds take away a fraction of locally accreting mass, i.e., we parametrize  $\dot{M}$  at the BH as (e.g., Blandford & Begelman 1999)

$$\dot{M} = \left(\frac{r_0}{r_D}\right)^\beta \dot{M}(r_D), \quad (11)$$

where  $r_0 = 10r_g$  is a characteristic radius at which the disk wind, which carries away mass from the disk, starts. The value of  $\beta$  controls the strength of mass loss:  $\beta = 0$  means no mass loss,  $\beta = 1$  means very strong mass loss. GR numerical simulations suggest  $\beta \approx 0.5$  (McKinney et al. 2012; Narayan et al. 2012).

We show the effects of disk mass-loss in Figures 8 and 9 for 3 different values of mass-loss parameter:  $\beta = 0, 0.5$ , and 1. Figure 8(a) shows that the presence of mass-loss suppresses BH mass accretion rate: the thick solid line, which corresponds to the case  $\beta = 0$  and does not include any mass loss (see eq. 11), lies above the other two lines for  $\beta = 0.5$  and 1, both of which include mass-loss. The suppression of  $\dot{M}$  for  $\beta > 0$  leads to the suppression of BH mass growth: as is clear from Fig. 8(a),(b), the higher the value of  $\beta$ , the stronger the mass loss, the smaller the BH mass. However, the plausible range of  $\beta$  we considered results in only a modest change in  $M_{\text{BH}}$ , by at most a factor of 2. Figure 8(c) shows that mass loss does not strongly affect BH spin, either: its value levels off at  $a \approx 1$  soon after jet breakout for the entire range of  $\beta$  considered. This is because by the time mass-loss becomes substantial (i.e.,  $r_D \gg r_0$ ), the BH was already spun up to a near-maximum spin,  $a \gtrsim 0.9$ .

Figure 9(a) shows that jet power,  $L_j \propto M_{\text{BH}}^2$ , is slightly increased for  $\beta > 0$ , due to the suppression of BH mass growth. Figure 9(b) shows that mass loss does not change the amount of magnetic flux brought to the BH, i.e., the three solid lines, each for a different value of the mass-loss parameter  $\beta$ , are on top of each other. This is to be expected, since in our model the time-dependence of  $\Phi_{\text{BH}}$  is determined by the initial distribution of magnetic flux in the progenitor star and therefore depends neither on mass-loss nor the choice of  $\beta$  (see eq. 11).

Whereas mass loss only weakly affects the GRB luminosity, it does affect the duration of the prompt emission: the larger the mass loss, the earlier the MAD onset, the shorter the GRB. Figures 8 and 9 indicate the MAD onset time with blue stars: for a stronger mass-loss (larger values of  $\beta$ ), the MAD forms at an earlier time. This is to be expected, since mass loss diminishes mass accretion rate and therefore BH magnetic flux, which remains unaffected by mass loss, becomes dynamically important at an earlier time.

Thus, all our previous conclusions hold in the presence of mass-loss. Summing up, jet power throughout the GRB duration is rather constant. The presence of mass-loss causes the remnant BH to be smaller, and therefore, for the same available magnetic flux the jet power to be slightly larger. Since mass-loss reduces  $\dot{M}$  at the BH, the disk turns MAD earlier and therefore the GRB duration is shortened. The effects of the mass-loss on GRB lightcurves are thus moderate at most.

### 3.4 Effect of Stellar Rotation

An important, but poorly understood, property of GRB progenitor stars is their rotation. There is observational indication of anti-

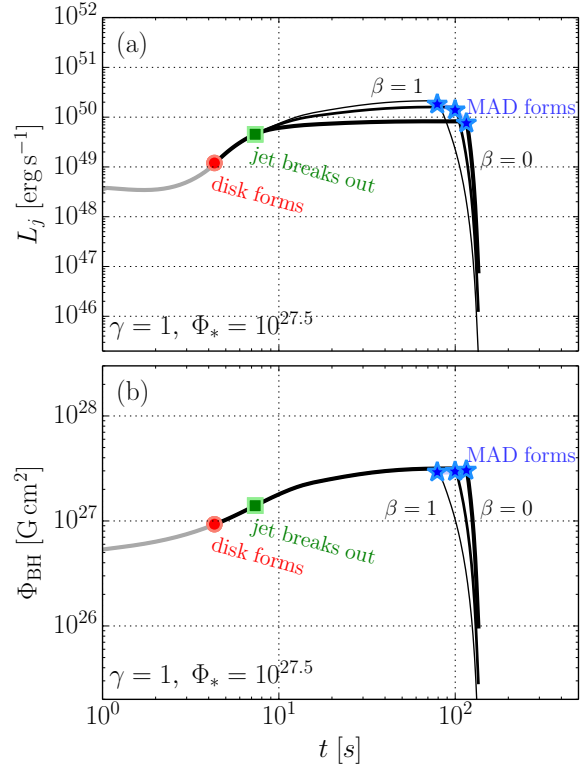


**Figure 9.** Similar to Fig. 8, but for  $\Phi_{\text{BH}}$  and  $L_j$ . The mass loss does not qualitatively affect the temporal dependence of jet power. However, it does change the duration of the prompt emission: the larger the mass loss, the earlier the MAD onset, the shorter the GRB.

correlation between stellar metallicity and the occurrence of GRBs (see, e.g., Modjaz et al. 2008). This can be understood if rapid rotation of progenitor is required for its core collapse to result in a GRB: higher metallicity leads to stronger stellar winds, which extract stellar angular momentum and slow down stellar rotation. In fact, there are many competing models, and the underlying physical processes are not agreed upon.

Motivated by this, we explore the effect of stellar rotation on the emergent GRB luminosity within our model. We started by varying the stellar rotation rate,  $\omega$ , by a constant factor relative to  $\omega_*(r)$ , the rotation rate in our fiducial model. Figure 10(a) shows the analog of Fig. 6(a) computed for  $\omega = 0.23\omega_*$ . The decrease in stellar rotation causes the jet to break out at a much later time. This is because the lower angular momentum of the stellar envelope means that most of the star collapses into a BH directly, bypassing the formation of an accretion disk. Since we assume that the presence of an accretion disk is required for the production of jets (see Sec. 2.1), the formation of the disk and jets does not take place until much later and can lead to a much shorter duration of the GRB. For instance, in our fiducial model, disk (and jet) formation takes place  $\sim 10$  s after the core collapse (see Fig. 6a), and the duration of the GRB is comparable to the stellar free-fall time, or  $\approx 100$  s. However, for  $\omega = 0.23\omega_*$ , the disk forms at a much later time,  $\approx 56$  s after the core collapse and jet breaks out at  $\approx 61$  s (somewhat later for weaker  $\Phi_*$ , as seen in Fig. 6). The duration of the GRB is reduced, down to 57 s. Thus, the slower the stellar rotation, the shorter is the GRB. For very slow stellar rotation, this effect would prevent the standard GRBs from happening altogether: the

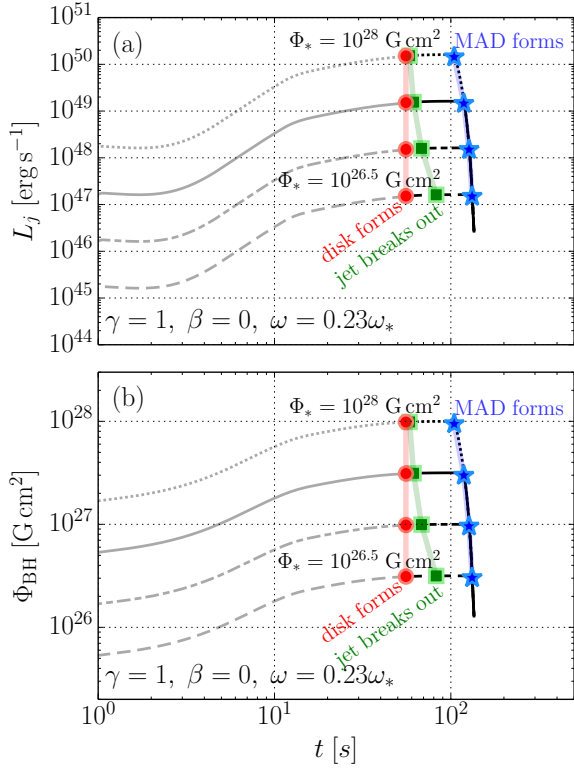


**Figure 10.** Jet power and magnetic flux vs. time, for slower stellar rotation than in our fiducial model ( $\omega = 0.23\omega_*$ ) and different values of magnetic flux in the progenitor star,  $\Phi_*$ . Comparison to Fig. 6 shows that slower rotation does not noticeably affect the power of the jets. However, it does lead to a later time of debris circularisation and disk formation (shown with red circles) and jet breakout (shown with green squares that are barely visible under the red circles). Since the time of MAD formation (shown with blue stars) stays the same, slower rotation of a progenitor leads to shorter GRBs.

GRB starts in the steep decay stage and might instead appear as a low-luminosity GRB, as we discuss below.

The above example makes it clear that the standard GRB lightcurve profile is extremely resilient, even when the stellar rotation is extremely slow: the jet power follows a plateau, which abruptly ends in a steep decline. It could be a concern that the presence of large-scale magnetic field in a progenitor star might lead to the slow-down of the stellar core by magnetic torques and even potentially result in solid-body-like rotation of the star as a whole. Can GRBs be produced in such an unfavourable scenario?

To explore this, we consider solid-body rotation in the progenitor star, with a constant angular velocity,  $\omega = \text{constant}$ . We choose the rotation rate such that the surface layers of the star rotate at 10% of Keplerian value, which corresponds to surface rotational velocity  $v_* \approx 200 \text{ km s}^{-1}$ . As Fig. 12(a) illustrates, the mass accretion rate is unaffected by the rotation profile (c.f. Fig. 3a). Since for solid-body rotation most of the angular momentum is carried by the outer layers of the star, the collapse of the core leads to essentially a non-spinning BH,  $a(t = 1 \text{ s}) \approx 0.003 \ll 1$  (see Fig. 12b), which is too low a spin to power a jet of substantial power. Thus, naively, it would seem that this scenario is hopeless for producing a GRB!

However, this is not so: just as we saw above in the case of slow rotation, the GRB does not start until the infalling gas hits the centrifugal barrier and forms an accretion disk and a jet. In this model, this happens around  $t \approx 57 \text{ s}$  (marked with red circle in

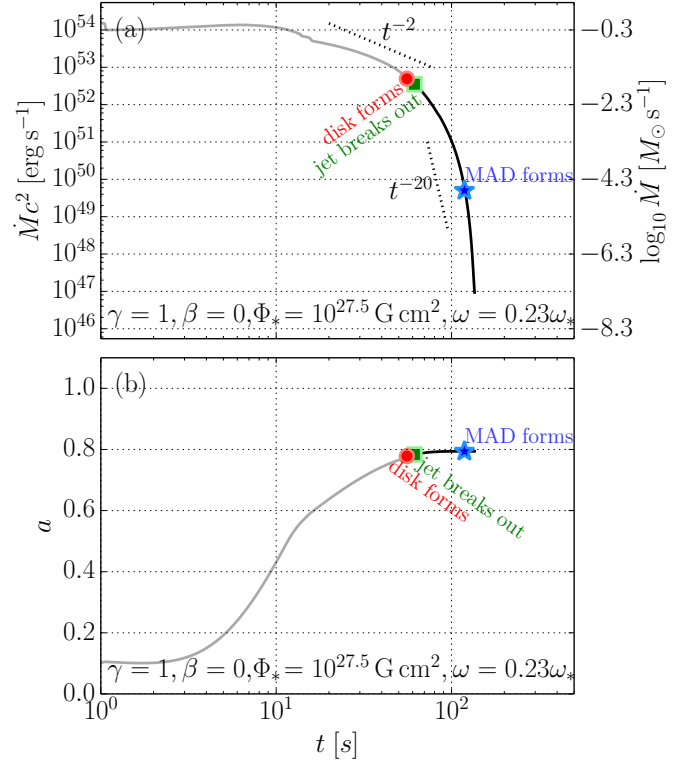


**Figure 11. [Panel (a)]:** The slower rotation of the progenitor star (23% of our fiducial model), does not lead to any changes in mass accretion rate:  $\dot{M}$  is the same as in our fiducial model, see Fig. 3(a). **[Panel (b)]:** Despite the progenitor star has only 23% of the angular momentum of our fiducial model, the collapse leads to a rapidly spinning BH, with  $a \approx 0.8$ . The rather high spin leads to BH power similar to our fiducial model. The primary effect of the slower rotation is the delay of disk and jet formation, which results in a shorter GRB.

Fig. 12a), and the jet breaks out of the star and the GRB starts at  $t \approx 76 \text{ s}$  (indicated by the green square). By this late time, the central BH receives most of the angular momentum carried by the outer layers of progenitor star, and BH spin saturates at a respectable value,  $a \approx 0.4$ . Jet power, shown in Fig. 13(a), and BH magnetic flux, shown in Fig. 13(b), saturate at near-constant values standard for GRBs:  $L_j \lesssim 10^{50} \text{ erg s}^{-1}$  and  $\Phi \sim 10^{27} \text{ G cm}^2$ . The end of the GRB is marked by the onset of MAD and occurs at approximately the same time as in our fiducial model,  $t_{\text{MAD}} \approx 100 \text{ s}$ . Thus, the duration of the GRB is shortened down to  $\approx 40 \text{ s}$  from  $\approx 100 \text{ s}$  in our fiducial model.

Thus, the details of radial distribution of angular momentum inside the star are not important for the observational appearance of the GRB: for instance, GRB light curves are essentially identical for the slow stellar rotation, with  $\omega = 0.23\omega_*$  (see Fig. 11) and the case of solid-body rotation, with  $v_* = 200 \text{ km s}^{-1}$  (see Fig. 12). The only major underlying difference is that the latter results in an approximately twice as low BH spin and therefore a somewhat shorter GRB. For instance, for the weakest stellar magnetic flux value we considered,  $\Phi_* = 10^{26.5} \text{ G cm}^2$ , the jet does not break out of the star at all (see Fig. 12a,b) and thus no normal GRB is produced. Therefore, for a normal GRB to occur, it is important to have both sufficient stellar magnetic flux and stellar angular momentum.

The slower the rotation, the shorter the GRB duration. As the angular momentum of the progenitor is reduced, the duration of

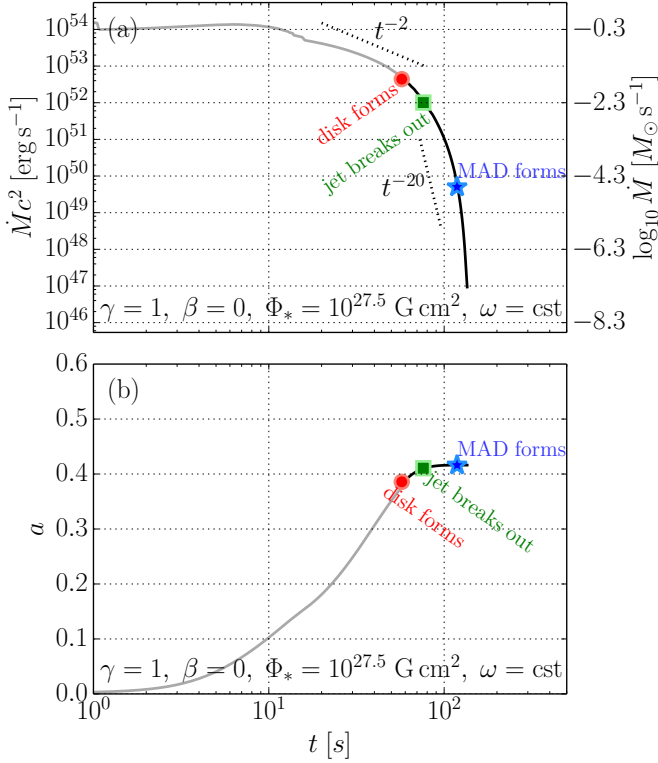


**Figure 12.** GRB properties vs time for a model with a *solid-body rotation* profile in the progenitor star, with surface rotation speed of  $200 \text{ km s}^{-1}$ , which is a characteristic rotational speed for O-stars. **[Panel (a)]:** Time-dependence of  $\dot{M}$  for a progenitor star with a solid-body rotation profile.  $\dot{M}(t)$  is the same as in our fiducial model, but disk formation and jet break-out happen at a later time due to the lower angular momentum of the progenitor star (compared to Fig. 3). **[Panel (b)]:** BH spin,  $a$ , vs time. Because for solid-body rotation  $\ell \propto r^2$ , most of the angular momentum resides in the outer layers of the star and reaches the BH late in the course of the core-collapse; in fact, direct collapse into BH of the core leads to an essentially non-rotating BH:  $a \approx 3 \times 10^{-2}$  at  $t \approx 1 \text{ s}$ . However, by the time the accreting material hits the centrifugal barrier and circularises,  $t \approx 60 \text{ s}$ , BH spin reaches a respectably high value,  $a \approx 0.4$ .

a core-collapse GRB can become shorter than  $\approx 2 \text{ s}$ , which is the standard divide between the populations of short- and long-duration GRBs (Kouveliotou et al. 1993). This can make long-duration GRBs appear as short GRBs (see also Bromberg et al. 2012, 2013). For very slow rotation, the jets either barely have enough time to break out of the star or fail to break out of the star and can result in a low-luminosity GRB or an X-ray flash. If the analogy with low-luminosity GRBs holds, such a failed or near-failed GRB can be accompanied by a supernova explosion (Stanek et al. 2003; Modjaz et al. 2006).

So far we have assumed that for the jet to form, the accreting material needs to hit a centrifugal barrier. What happens if the gas never hits the centrifugal barrier and the disk does not form? In such a limit of very slow rotation, it might seem that the jet never forms and there would be no GRB at all, as without the disk, there is no low-density funnel through which the jet can escape. However, this is not the case. In fact, the low-density funnel is only a necessity for jet formation when the magnetic field is *not* dynamically-important. However, once a MAD forms, a jet will be produced even by a non-rotating accretion flow in the absence of a low-density funnel (Komissarov & Barkov 2009; Tchekhovskoy

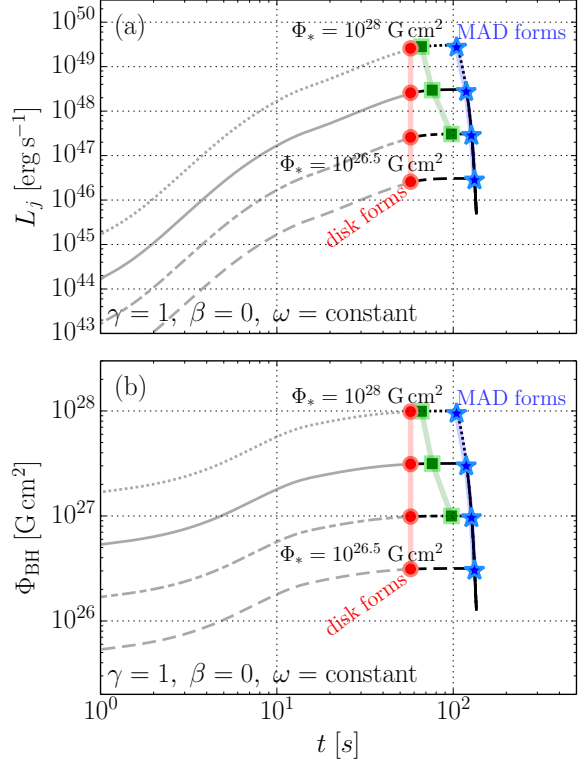


**Figure 13.** GRB properties vs time for a model with a *solid-body rotation* profile in the progenitor star, with surface rotation speed of  $200 \text{ km s}^{-1}$ , which is a characteristic rotational speed for O-stars. **[Panel (a)]:** GRB luminosity vs time for different values of stellar magnetic flux, as labeled (see also Fig. 6). The relatively modest solid-body rotation leads to a delayed formation of disk and jet: around  $60 \text{ s}$  post-collapse. Despite this delay, the lightcurve follows the standard GRB template, with a constant-luminosity plateau lasting about  $40 \text{ s}$  (shorter for weaker magnetic flux) and followed by an abrupt turn-off. For the weakest magnetic flux,  $\Phi_* = 10^{26.5} \text{ G cm}^2$ , the jet is so weak that it does not make it out of the star before the accretion turns off. **[Panel (b)]:** BH magnetic flux  $\Phi_{\text{BH}}$  as function of time, for different values of total stellar magnetic flux,  $\Phi_*$ . The magnetic flux time-dependence is identical to that in our fiducial model shown in Fig. 6(b). Thus, the primary effect of the solid-body rotation is the delayed time of disk and jet formation and shortening of the GRB duration.

et al. 2014). We estimate that the energetics of such events is of order  $L_{\text{MAD}} t_{\text{MAD}}/20$ , or about 5% of the energetics of normal GRBs. (Here the factor of  $1/20$  comes from integrating the luminosity time-dependence  $L_j \propto t^{-20}$  around the onset of the MAD regime.) Thus, on the energetics grounds it is conceivable that such events could indeed be the counterparts of low-luminosity GRBs.

Summarising, GRBs appear to be successfully produced over a wide range of progenitor rotation rates and profiles. The lower the angular momentum of the progenitor star, the shorter is the GRB that results. However, regardless of the progenitor rotation rate and profile, GRBs robustly show an early-time plateau followed by the sharp decline. Thus, the observational appearance of GRBs appears to be insensitive to the details of angular momentum distribution inside the progenitor star. How do other parameters of the progenitor affect the GRB?

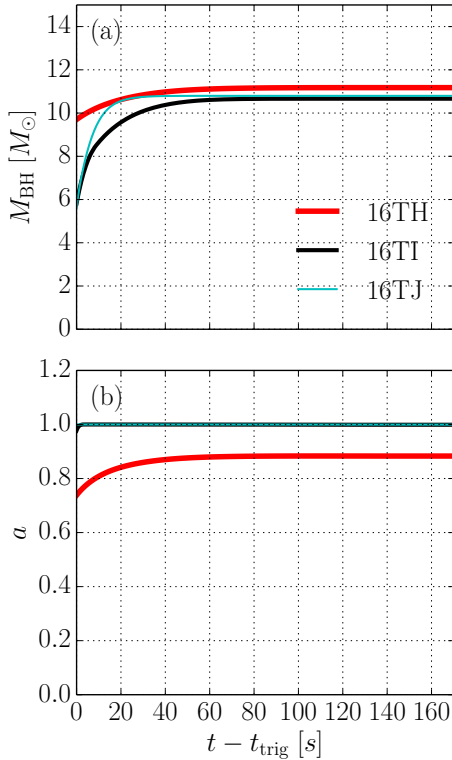


**Figure 14.** BH mass and spin vs. time since the trigger for different stellar progenitor models: 16TH (thick solid red lines), 16TI (medium-thickness solid black lines), and 16TJ (thin cyan lines). In all cases, we use our fiducial model parameters:  $\gamma = 1, \beta = 0, \Phi_* = 10^{27.5}$ . Panel (a) shows that BH mass change is between 10% for model 16TH and 50% for models 16TI and 16TJ. BH spin remains approximately constant in time (to better than 20%) and levels off to a high value:  $\approx 0.9$  for model 16TH and  $\approx 1$  for models 16TI and 16TJ.

### 3.5 Effect of Stellar Progenitor Model

We will now investigate the effect of the pre-collapse stellar model on GRB light curves. For simplicity, in all cases we choose our fiducial parameters:  $\gamma = 1, \beta = 0$  (=no mass loss), and  $\Phi_* = 10^{27.5}$ . Figure 14 shows the time-dependence of BH mass (panel a) and spin (panel b) for 3 different progenitor models: 16TH, 16TI and 16TJ. The temporal profiles of  $M_{\text{BH}}$  and  $a$  are qualitatively similar in all 3 models: both mass and spin level off early in the course of the GRB and do not change thereafter. In all models BH spin ends up at a rather high value,  $a \gtrsim 0.9$ .

Figure 15(a) shows that  $\dot{M}$  drops by several orders of magnitude during the GRB. However,  $\dot{M}$  does not directly control jet power,  $L_j$  (see Sec. 2.2.2). For this reason,  $L_j$ , remains mostly constant throughout the GRB, as is clear from Fig. 15(b). All 3 progenitor models lead to virtually indistinguishable shapes of prompt emission light curves: all of them show about 50% variation at the very beginning of the GRB, after which the emission levels off to a constant. In all cases, at the end of the GRB, the jet power abruptly drops. This happens when  $\dot{M}$  drops below  $\dot{M}_{\text{MAD}}$  (see eq. 4), after which jet power begins to track the rapidly decreasing mass accretion rate. The durations of the GRBs for the 3 different stellar models we have considered are within a factor of 2 of each other and in all cases are set by the free-fall time scale of the outer layers of the progenitor star.

In summary, all basic properties like  $M_{\text{BH}}$ ,  $a$ , and  $\dot{M}$  do not dif-

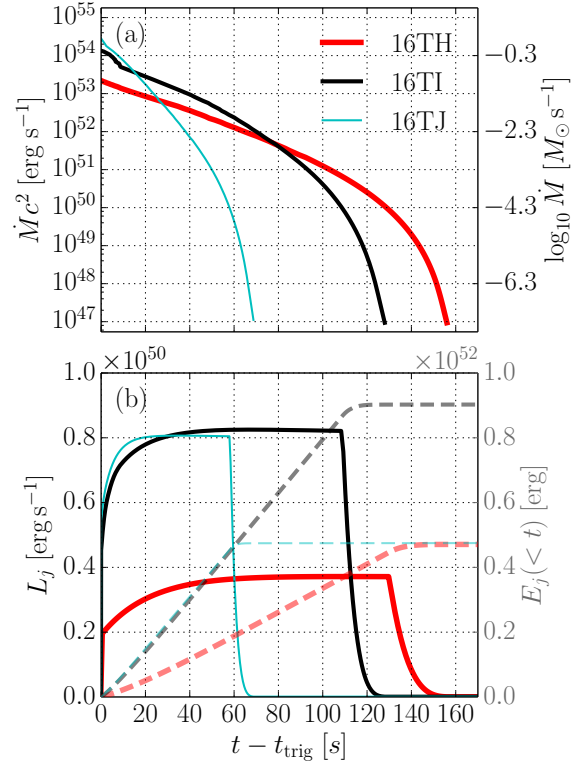


**Figure 15.** Time-variation of various quantities for different stellar progenitor models (see the legend and caption to Fig. 14 for details). In all cases, we use our fiducial model parameters:  $\gamma = 1, \beta = 0, \Phi_* = 10^{27.5}$ . **[Panel (a)]:** shows mass accretion rate  $\dot{M}$  on a *logarithmic scale*: it changes by many orders of magnitude during the GRB and differs from one model to another by 1 – 2 orders of magnitude. **[Panel (b)]:** Solid lines show the power of the jets  $L_j$  on a *linear scale*. In contrast to  $\dot{M}$ , the power remains relatively constant and changes between the models by at most a factor of 2. This is because during the GRB, jet power is decoupled from the widely varying mass accretion rate. To help us visually quantify the constancy of  $L_j$ , the lighter-coloured dashed lines and the right y-axis show cumulative light curves of jet power,  $E_j(<t) = \int_0^t L_j dt'$ , for the three models. That  $E_j(<t)$  shows little curvature throughout the prompt emission is a reflection of the near-constancy of its slope, or jet power.

fer substantially between different stellar models. For a fixed magnetic flux through the progenitor,  $\Phi_*$ , the jet power  $L_j$  differs by factors of just a few. The magnetic flux therefore appears to be the only quantity that can feasibly account for the huge range of observed GRB luminosity. Note, however, that the progenitor properties such as rotation can have an effect on the GRB duration (Sec. 3.4) and may have an indirect effect on the field strength (e.g. the faster rotators can have stronger magnetic fields). Since the origin of stellar magnetism is not well-understood, we do not explore such cross-correlations in this work.

## 4 COMPARISON WITH GRB LIGHTCURVES

The GRB emission is made up of a superposition of many pulses. The pulse properties, such as peak flux, duration, inter-pulse intervals, do not change in any systematic way during the burst. As a result, cumulative photon counts during GRBs increase, on average, linearly with time:  $\int_0^t L_{\gamma} dt \sim \text{constant} \times t$  or  $L_{\gamma} \sim \text{constant}$

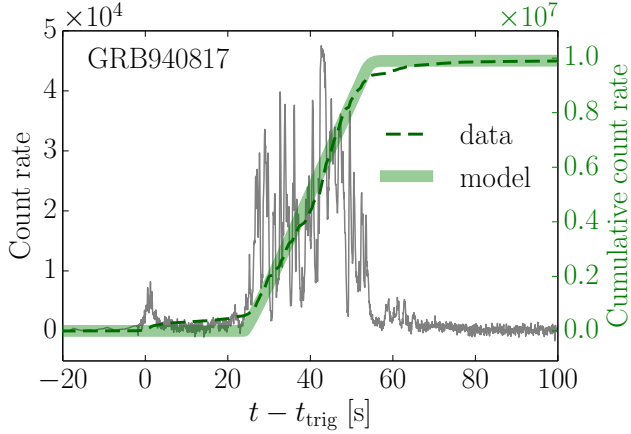


**Figure 16.** BATSE X-ray lightcurve (in all channels combined) for GRB 940817 is shown with solid grey line (left y-axis). The cumulative light curve is shown with dashed green line (right y-axis). Light green stripe shows the model-predicted cumulative lightcurve for progenitor 16TI (Woosley & Heger 2006) and the magnetic flux distribution index of  $\gamma = 1$ .

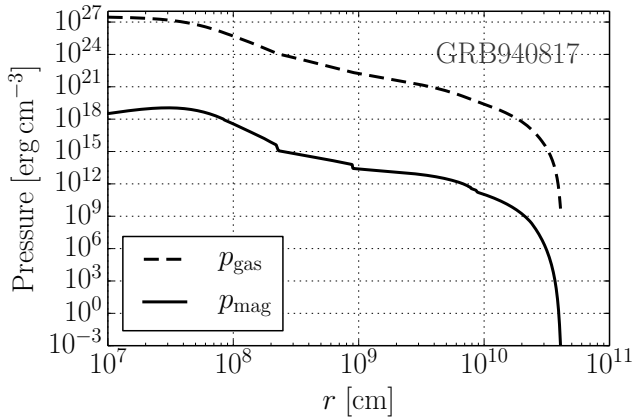


**Figure 17.** The radial profile of gas and magnetic pressures corresponding to Fig. 16.

(McBreen et al. 2002). Here we show that our model reproduces this observation.

In Fig. 15(b) we plot along the right y-axis the cumulative light curves of our simulated GRBs with dashed lines. The cumulative light curves are mostly straight lines throughout the prompt emission, indicating the near-constancy of jet power. We will now apply this type of visual analysis to several representative BATSE light curves.

McBreen et al. (2002) demonstrated that the cumulative count rate increases linearly with time in a sample of  $\sim 500$  bright BATSE bursts. Here we repeat their analysis for representative GRBs, 940817, 940210, 920513, and compare the results to the predictions of our model.

We chose GRBs 940817 and 940210 because they are rather clean examples of the linear increase of the radiated energy versus time followed by a sharp turn-off of the GRB emission. In Figs. 16 and 18 we overplot the cumulative count rate from these bursts with those for our model (we rescaled the time axis to fit the observed duration). We adopt our fiducial model parameters: the magnetic flux distribution index of  $\gamma = 1$ , the total magnetic flux of  $\Phi_* =$

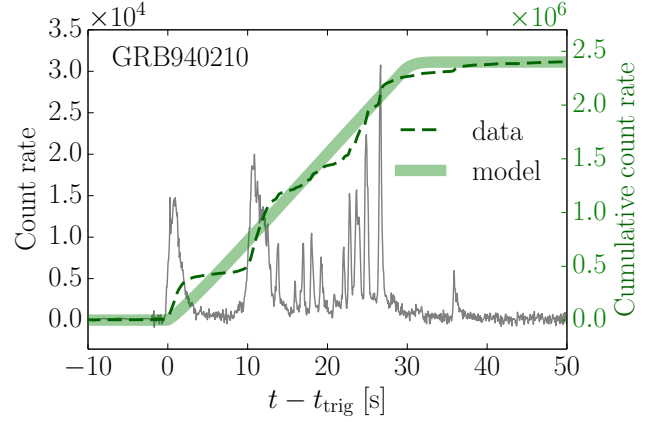


**Figure 18.** BATSE X-ray lightcurve (in all channels combined) for GRB 940210 is shown with solid grey line (left y-axis). The cumulative light curve is shown with dashed green line (right y-axis). Light green stripe shows the model-predicted cumulative lightcurve for progenitor 16TI (Woosley & Heger 2006) and the magnetic flux distribution index of  $\gamma = 1$ .

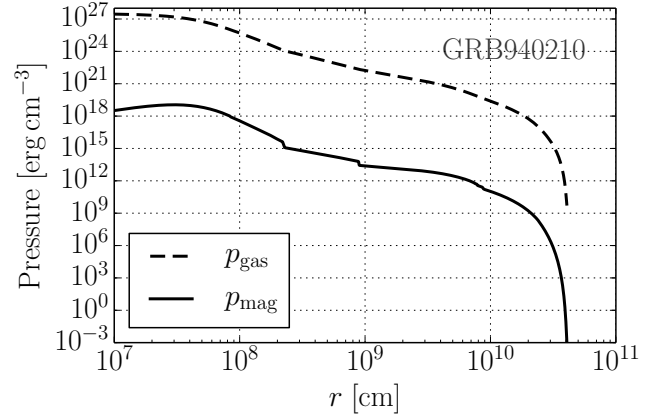


**Figure 19.** The radial profile of gas and magnetic pressures corresponding to Fig. 18.

$10^{27.5}$  G cm<sup>2</sup>, no mass-loss from the disk ( $\beta = 0$ ), along with the 16TI progenitor star model. The results for other combinations of model parameters,  $\gamma$ ,  $\beta$ , and  $\Phi_*$ , and progenitor models are similar (not shown).

As is illustrated by Figs. 16 and 18, our models naturally account for the near constancy of the burst luminosity over its duration as well the steep decline of the jet power at  $t - t_{\text{trig}} \sim 60$  s and 30 s, respectively. For comparison, in Figs. 17 and 19 we show the implied gas and magnetic pressures as functions of distance in the pre-collapse star for the same two models. The gas pressure dominates magnetic pressure in the star by a typical factor of  $\sim 10^9$ .

#### 4.1 Magnetic tomography of progenitor stars

From Fig. 20 it is clear that gross properties of the cumulative count rate from GRB 920513 can also be reproduced by this simplest version of the model. However, the cumulative light curve has either a pronounced bump at  $t - t_{\text{trig}} \sim 40$  s or a deficit at  $t - t_{\text{trig}} \sim 60$  s.

Such a deviation from the simple prescription where magnetic flux scales with mass in the progenitor star can be used as a probe

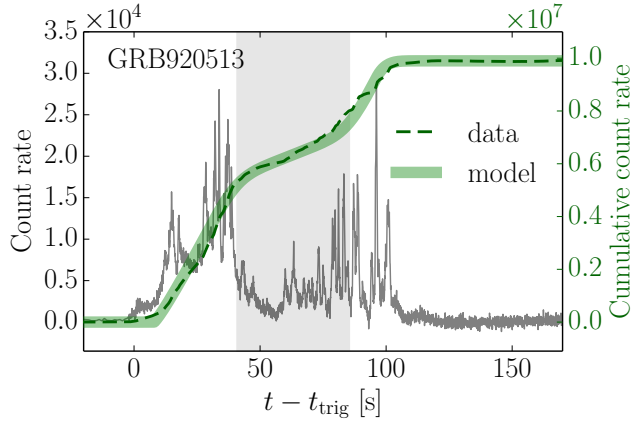


**Figure 20.** BATSE X-ray lightcurve (in all channels combined) for GRB 920513 is shown with solid grey line (left y-axis). The cumulative light curve is shown with dashed green line (right y-axis). Light green stripe shows the model-predicted cumulative lightcurve for progenitor 16TI (Woosley & Heger 2006) and the magnetic flux distribution index of  $\gamma = 1$ . To model the suppression of power in the second half of the GRB, we added a torus-like magnetic field component centred at  $t - t_{\text{trig}} = 70$  s and indicated with the vertical grey stripe. The magnetic field in the inner part of the torus is of opposite polarity to that in the rest of the star. Hence, the accretion of the torus causes a temporary suppression of GRB power.

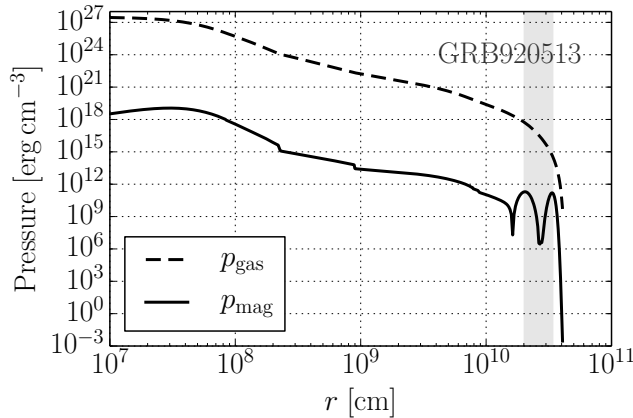


**Figure 21.** The radial profile of gas and magnetic pressures corresponding to Fig. 20. For this burst, we added an additional magnetic torus of opposite polarity to that in the rest of the star. This component is centred at  $t - t_{\text{trig}} \sim 60$  s (approximately at  $r \sim 3 \times 10^{10}$  cm), with the width of  $\sim 20$  s (approximately  $10^{10}$  cm), and indicated with the vertical grey stripe. It appears as two bumps in the magnetic pressure profile (see Fig. 20 and text for details).

of the stellar field structure. To account for the relative weakness of the burst at the interval  $50 \leq t \leq 80$  s, we introduce an additional torus-shaped component of poloidal magnetic field centred at  $t - t_{\text{trig}} \sim 60$  s, or a distance  $r \sim 3 \times 10^{10}$  cm in the progenitor star. This component appears in Fig. 21 as a pair of bumps in the magnetic pressure and is indicated by a vertical grey band. Namely, we superimpose on top of our  $\gamma = 1$  magnetic flux profile a magnetic “knot”: a torus-like poloidal magnetic field component of negative polarity, such that the consumption by the BH of this knot temporarily depresses BH magnetic flux. We take the time-dependence

of BH magnetic flux of the following form:

$$\Phi_{\text{BH}}^{\text{GRB920513}}(t) = \Phi_* \left( \frac{M_{\text{collapsed}}}{M_*} \right) \left\{ 1 - f_0 \exp \left[ - \left( \frac{t - t_{\text{trig}} - t_0}{\Delta t_0} \right)^4 \right] \right\}, \quad (12)$$

where the term in the curly braces represents BH magnetic flux suppression factor. For illustration, we performed a by-eye fit and obtained the following parameters  $f_0 = 0.55$ ,  $t_0 = 63$  s, and  $\Delta t_0 = 23$  s. Here,  $f_0$  is a dimensionless parameter equal to the dimensionless magnetic flux carried by the knot, i.e., the ratio of the magnetic flux in the knot to the net flux in the star. Thus,  $f_0 = 1$  means that, as the knot is consumed by the BH, the jet power vanishes completely, a value of  $f_0 \lesssim 1$  leads to a substantial suppression of BH magnetic flux and GRB luminosity, whereas  $f_0 \ll 1$  leads to a small dip in the flux and luminosity.

When the inner half of the magnetic knot accretes ( $t - t_{\text{trig}} \sim t_0 - \Delta t_0 = 40$  s), the total BH magnetic flux gets reduced by a factor of  $(1 - f_0)^{-1} \approx 2$  and the jet power by a factor of  $(1 - f_0)^{-2} \approx 5$ . Subsequent accretion of the outer half of the knot (at  $t - t_{\text{trig}} \sim t_0 + \Delta t_0 = 86$  s) replenishes the BH magnetic flux and leads to the recovery of jet power. Note that the magnetic knot fully resides under the stellar surface and so does not affect the surface magnetic field strength.

GRB 940210 lightcurve shows two prominent deficits, or quiescent intervals, as seen in Fig. 18: one at  $t - t_{\text{trig}} \sim 5 - 10$  s and another one at  $t - t_{\text{trig}} \sim 15 - 20$  s. Similar to GRB 920513, we can model these quiescent intervals by introducing magnetic knots into an otherwise large-scale magnetic flux distribution in the star. As each magnetic knot is accreted by the BH, the knot’s magnetic flux cancels out a substantial fraction of BH magnetic flux and leads to a depression in GRB luminosity. We model the magnetic flux in the knots similar to eq. (12):

$$\Phi_{\text{BH}}^{\text{GRB940210}}(t) = \Phi_* \left( \frac{M_{\text{collapsed}}}{M_*} \right) \times \prod_{i=1,2} \left\{ 1 - f_i \exp \left[ - \left( \frac{t - t_{\text{trig}} - t_i}{\Delta t_i} \right)^4 \right] \right\}. \quad (13)$$

Here we choose  $f_1 = 0.85$ ,  $t_1 = 6.1$  s,  $\Delta t_1 = 2.9$  s, and  $f_2 = 0.55$ ,  $t_2 = 18.6$  s,  $\Delta t_2 = 3.9$  s (we give the precise values for reproducibility; however, qualitative behaviour of the lightcurve is insensitive to the details of the fit). Thick green line in Figure 22 shows the predicted cumulative GRB lightcurve with the thick solid green line: the accretion of magnetic knots, which are indicated by grey vertical stripes in Figs. 22 and 23, leads to the partial depressions in BH magnetic flux and in turn to quiescent intervals in jet power, similar to those seen in GRB lightcurves.

More generally, we suggest that rather long periods of silence between bursts of prompt emission, such as in the case of GRB 940210 and GRB 920513, could be an imprint of large-scale magnetic field inhomogeneities in the progenitor star. This opens up the possibility of stellar magnetic flux “tomography”: inferring the magnetic flux distribution in progenitor stars by inverting the information contained in their GRB light curves, as we have illustrated for GRB 920513 and GRB 940210.

Note that, as seen in Fig. 22, the GRB power does not strongly change from one interval of activity to another (i.e., the cumulative light curve slope is approximately the same among all active intervals). But it changes from one quiescent interval to another (cumulative light curves have different slopes in different quiescent intervals). This behaviour is common to many GRBs (McBreen et al. 2002), and our model provides a natural explanation for this: GRB power during quiescent intervals depends on the magnetic flux in the knots, whereas the power during active intervals is set by the

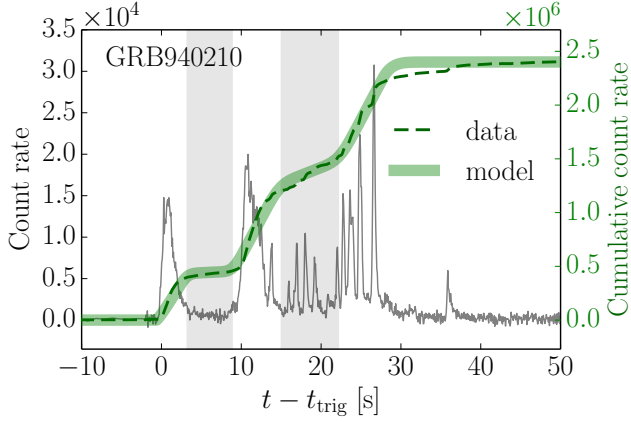


**Figure 22.** Similar to Fig. 18 but with the addition of two magnetic knots, which are centred at  $t - t_{\text{trig}} \sim 5$  s and  $\sim 20$  s and indicated by vertical grey stripes and containing magnetic fluxes that make  $\sim 85\%$  and  $\sim 55\%$  that through the star. Stellar magnetic flux distribution versus radius is given by eq. (13). As these knots are consumed by the BH, BH magnetic flux and GRB power are depressed.

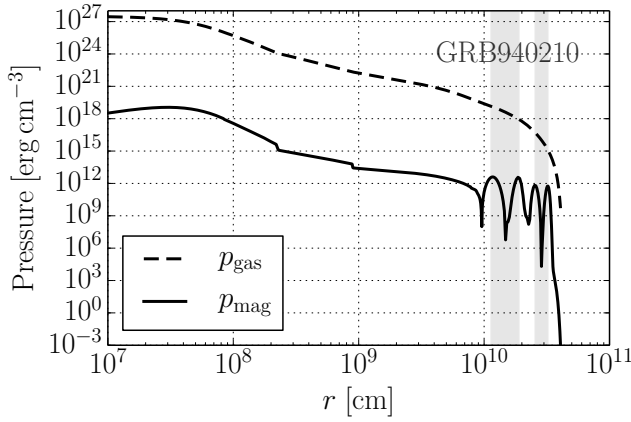


**Figure 23.** The radial profile of gas and magnetic pressures corresponding to Fig. 22. Each of the two magnetic knots is seen as a pair of bumps on top of the underlying, monotonically decreasing magnetic pressure profile (which is shown in Fig. 19). Vertical grey stripes indicate the one-sigma extent of the knots that matches the extent of the bumps in magnetic pressure.

net magnetic flux through the star and is therefore roughly constant throughout the GRB. This is consistent with suggestions (Nakar & Piran 2002) that quiescent intervals follow a different type of time-variability than (i) short time-scale, pulse-to-pulse variability of GRBs and (ii) long time-scale variability set by the duration of the GRB. Within our model, the latter is set by the free-fall time-scale of the outer layers of the star. The former could be caused by, e.g., the emission mechanism (Kumar & Narayan 2009; Narayan & Kumar 2009), jet propagation effects (Morsony et al. 2010), or the variability of the central engine. We discuss these possibilities in more detail at the end of this section.

In both cases of GRB 920513 and GRB 940210 the values of the  $f$ -factor (see eqs. 12 and 13), which sets the depth of the dip in the light curve due to the accretion of a magnetic knot, are of order of unity. This is precisely what is needed for the quiescent interval to be noticeable: in order to substantially modify the light curve, the knot must contain a magnetic flux comparable or larger

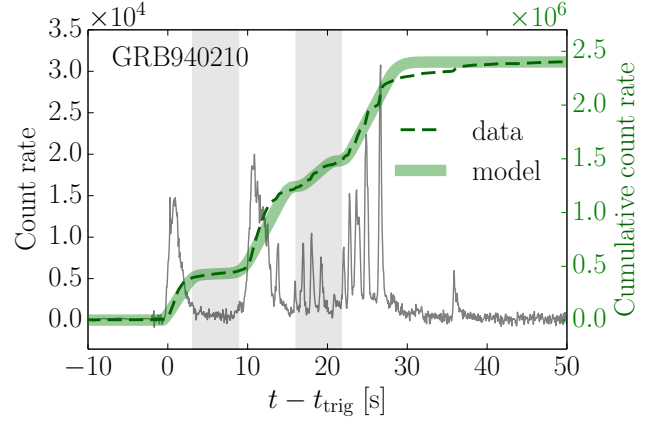


**Figure 24.** Similar to Fig. 22 but with the two knots containing magnetic fluxes that make up 85% and 160% of those through the star (see text for details). Note the qualitative difference from Fig. 22 in which the knots contain 55% and 85% of that through the star: here we have a flux of 160% > 100%, which leads to “flat–steep–flat” behaviour of the cumulative light curve. This behaviour appears to be well-captured by our model (see text for details).

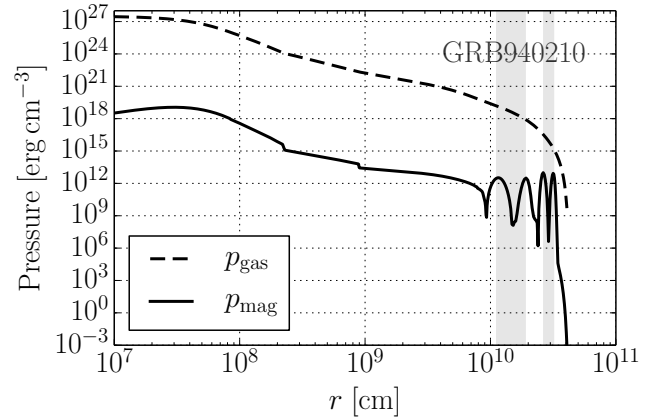


**Figure 25.** The radial profile of gas and magnetic pressures corresponding to Fig. 24. The magnetic pressure in the second knot is higher than that in Fig. 23, reflecting a larger magnetic flux contained in that knot.

than that on the BH,  $f \gtrsim 1$ . For this reason, it is surprising that for both of the above GRBs we find  $f < 1$ , i.e., the flux in the knot is lower than the net flux through the progenitor star. How does a knot know about the net magnetic flux through the star?

We tried and were unable to obtain a visually good fit to the GRB 920513 lightcurve with  $f > 1$ . The reason for this is clear. For a knot with  $f > 1$ , the magnetic flux on the BH would vanish twice: once at the beginning and once at the end of the consumption of the knot by the BH. This would lead to the cumulative GRB light curve that flattens at the beginning and at the end of the quiescent interval and steepens in between. No such behaviour is obviously present in Fig. 20: in fact, the cumulative light curve appears to rise continuously, suggesting that the knot that led to the quiescent interval in GRB 920513 light curve contained a relatively small magnetic flux compared to that on the BH. The situation is different with GRB 940210, whose light curve is shown in Fig. 22. The light curve appears to show precisely the type of behaviour indicative of a large flux in the knot, at least for the second quiescent interval of the two.

Indeed, we find that  $f_2 = 1.68 > 1$  gives a rather good fit to the cumulative light curve, as seen in Fig. 24, with the rest of the parameters similar to those used for the fit shown in Fig. 22:  $f_1 = 0.85$ ,  $t_1 = 6.2$  s,  $\Delta t_1 = 3.1$  s,  $t_2 = 18.7$  s, and  $\Delta t_2 = 3.1$  s. The difference in magnetic flux is reflected in Figure 25, which shows that the magnetic pressure in the second knot (indicated with the rightmost vertical grey stripe) is higher than in that in Fig. 23. The model with  $f_2 \approx 1.5$ , shown in Fig. 24, appears to give a visually better fit than that with  $f_2 \approx 0.5$ , shown in Fig. 22. This suggests that stellar magnetic inhomogeneities contain magnetic fluxes larger than the net flux through the star.

In the above, we assumed that the polarity of magnetic flux in the knots is negative, i.e., once a knot is accreted, it leads to a depression in BH magnetic flux and a quiescent interval in the GRB light curve. However, it is possible that in some cases the polarity of magnetic flux in the knots is positive. This then would lead to “hyper-active” intervals and substantial differences in GRB luminosity from one active interval to another. Statistical analysis of GRB light curves can potentially be used to determine the rates of occurrence of the two polarities of the magnetic knots, thereby providing us with valuable and otherwise not directly accessible information on the magnetic field structure inside of GRB progenitor stars.

So far we have considered magnetic flux inhomogeneities over two different scales inside the progenitor star: large-scales, comparable to  $r_*$  (net stellar flux), and smaller (but still large) scales, around  $0.1r_*$  (magnetic knots). It is conceivable that spatial distribution of stellar magnetic flux follows a continuous distribution. This spatial distribution of magnetic flux in a progenitor star leads to temporal distribution of quiescent intervals. Thus, temporal analysis of GRB lightcurves is warranted to constrain this distribution and thereby to improve our understanding of the geometry of magnetic fields in the progenitors of GRBs.

GRB light curves show variability over a wide range of time scales, from milliseconds to tens and hundreds of seconds. Until now, we have focused on how the properties of a GRB evolve on a timescale similar to its overall duration ( $t_{\text{GRB}} \sim 30$  s). We showed that the rotation of the star and the free-fall time of its outer layers set the GRB duration. We suggested that the spatial distribution of large-scale inhomogeneities of the magnetic field in the outer layers of the star leads to quiescent intervals in GRB light curves lasting  $\gtrsim$  few seconds. For completeness, here we speculate on what drives faster GRB variability, e.g., GRB pulses on  $t_p \lesssim 1$  s timescales. Such GRB variability may originate from the jet interactions with the stellar material. If the collapsing star is not axisymmetric, it can imprint perturbations, e.g., bends, onto the jet. Alternatively, if the jet is strongly magnetised, current-driven instabilities may lead to non-axisymmetric structures as the jet propagates through the star (Levinson & Begelman 2013; Bromberg et al. 2014a). Beaming effects can result in large temporal changes of the observed radiation even for modest changes of the Lorentz factor or the opening angle of the jet. Since the characteristic timescale for sound or Alfvén waves to cross the jet is  $\sim 1$  sec, short timescale variability may, in part, be due to the jet propagation through the collapsar.

Another process that may modulate the jet power on a short timescale is the excursions of the accumulated magnetic flux from the BH into the inner accretion disk and vice versa. The accretion disk may switch between a neutrino-cooled disk and a thick, advective disk multiple times during the GRB. Such transitions can have a profound effect on the jet power and GRB luminosity. Neutrino cooling results in a rather thin disk in the inner  $R_{\text{thin}} \sim 30r_g$  (Chen & Beloborodov 2007). When the inner disk is thin, most of

BH magnetic flux may diffuse outwards throughout  $R_{\text{thin}}$ , leaving only a small fraction of the magnetic flux on the BH and powering the jet. On the other hand, a thick disk can push most of the available flux into the BH, which can result in flares. Incidentally, the accretion timescale for the neutrino-cooled disk is a fraction of a second and may be of relevance for the typical duration of such gamma-ray pulses.

## 5 CONCLUSIONS

GRBs are characterised by the sudden onset of emission that lasts for  $T_{\text{GRB}} \sim 1$  min and is followed by a sharp turn-off. The time-averaged properties of the prompt emission such as luminosity do not show any clear systematic trends during the GRB. Within the collapsar framework, the trigger of the burst can be naturally associated with the moment at which the jet breaks through the surface of the collapsing star. The trigger takes place at time  $t_{\text{trigger}} \sim 10$  s after core collapse (MacFadyen & Woosley 1999; Bromberg et al. 2014b,a). Since  $T_{\text{GRB}} \gtrsim t_{\text{trigger}}$ , one expects that the accretion rate  $\dot{M}$  at the BH evolves (drops) appreciably over  $T_{\text{GRB}}$ . As a result, in any model for which the jet power directly depends on the accretion rate  $\dot{M}$ , one would expect the burst to become fainter throughout its duration until it is not detectable anymore. Such a behaviour is not observed.

Associating the gravitational energy release during the accretion onto the BH with the power of the GRB jets is hard on energetic grounds. Wolf Rayet stars have their masses varying over a narrow range. The black hole grows by several solar masses over the first minute past core collapse with the accretion power released  $\gtrsim 10^{54}$  erg. GRB jets, on the other hand, come in a broad range of energies  $\sim 10^{49-52}$  erg. Therefore, another parameter, and not the accreted mass, sets the GRB energetics and dispersion in their properties. We argue that this parameter is stellar magnetic flux.

To show this, we explored a number of models for collapsing Wolf-Rayet stars and demonstrated that, by the time the jet breaks through the collapsing star and the GRB becomes visible, the mass and spin of the BH are close to their asymptotic values, i.e.,  $M_{\text{BH}} \sim 10M_{\odot}$ ,  $a \approx 1$ , respectively. For reasonable assumptions about magnetic flux distribution in the star, the same holds true for the total magnetic flux  $\Phi_{\text{BH}}$  at the BH. Since the jet power in the Blandford-Znajek model depends only on these 3 weakly changing parameters ( $M_{\text{BH}}$ ,  $a$ ,  $\Phi_{\text{BH}}$ ), this explains the rough constancy of GRB luminosity during the burst.

But what causes the sharp turn-off of the GRBs? Since mass accretion rate decreases asymptotically to zero, eventually, the accretion rate drops to such a low level that the disk cannot confine the BH magnetic flux anymore. Then, the flux diffuses out into the disk, and the disk enters the *magnetically-arrested disk* (MAD) state (see Sec. 3.2). In MADs, jet power is proportional to mass accretion rate, and the jet power drops fast with time as  $L_j \propto \dot{M} \sim t^{-2 \dots -20}$ . Thus, it is the transition to the MAD regime causes the abrupt turnoff of the GRBs seen with *Swift*.

What leads to the large burst-to-burst variation of GRB luminosity? In our model, the jet power is set by the magnetic flux available in the progenitor star. Typical BH magnetic flux of  $\Phi_{\text{BH}} \sim 10^{27.5}$  G cm<sup>2</sup> is required to account for the observed luminosity of bright bursts, which implies a progenitor with surface magnetic field strength of  $B \sim 10^4$  G. Given the large observed variation in surface stellar magnetic field strength, it is conceivable that  $\Phi_{\text{BH}}$  varies by a factor of  $\gtrsim 30$  between different progenitors, and since jet power scales as  $\Phi_{\text{BH}}$  squared, such a variation translates

into 3 orders of magnitude variation in jet power, which is more than sufficient to account to the full observed range of GRB luminosities.

In addition to power, the GRBs show a large variety in their durations, from a few to a hundred seconds. What can cause such diversity? In our model, the GRB starts at the jet break out time and ends abruptly when the disk enters the MAD state. The jet breakout time is controlled by the longest of disk formation and jet propagation times. In most cases, it takes  $\sim$ ten seconds for the disk to form, which sets the trigger time, after which the GRB is detectable. It takes longer for the disk to form in progenitor stars with slow rotation. In such cases, the formation of the disk (and jet) can be substantially delayed, by tens of seconds, thereby shortening the GRB duration. Other than that, the slow rotation does not leave noticeable imprint on the GRB light curves, thus core-collapse GRBs with durations much shorter than the free-fall time of the outer layers of the progenitor star (which is around 100 s), might be suggestive of low angular momentum of their progenitors.

What can cause slow stellar rotation? One possibility is that magnetic torques couple the rotation of different layers inside the star, slow down the rotation of the core and potentially lead to near solid-body rotation of the progenitor, with the outer layers of the star carrying most of the stellar angular momentum. We showed that even such an extreme scenario can be capable of leading a long-duration GRB, suggesting that GRBs can be more robust than previously thought. Thus, in order to get a successful long-duration GRB, the progenitor star needs to contain sufficient angular momentum for the accretion flow to encounter a centrifugal barrier and spin up the central BH to a moderate spin. If high metallicity is conducive to the production of strong stellar winds, which remove stellar angular momentum, low stellar metallicity might be conducive to the production of long-duration GRBs. In the limit of extremely low stellar angular momentum, infalling stellar material does not encounter a centrifugal barrier, and an accretion disk does not form. In this scenario, the jet forms just before the onset of MAD, and we suggest that such extreme cases can be counterparts of failed or low-luminosity GRBs. These considerations may indicate that the flux through the progenitor is at least as a decisive factor for a successful GRB as the rotation of the collapsing star.

The MAD formation time (=the time at which GRB ends) is very close to the free-fall time of the outer layers of the star. Thus, another factor that controls the GRB duration is the radius of the progenitor star, with larger stars leading to longer GRBs. In this work, we neglected the effects of accretion disk formation on the GRB duration, which we estimate are insignificant, unless stellar rotation makes up a substantial fraction of Keplerian velocity. If the stellar rotation is near-Keplerian, an accretion disk of a large size and long accretion time can form, thereby extending the central engine activity time beyond the free-fall time of the outer layers of the star.

We used our model to probe the structure of the magnetic flux in the star. By fitting the lightcurve of GRB 949817, we infer that the total magnetic flux through the BH varies little throughout the burst. The same conclusion holds for the majority of bright GRBs that exhibit approximately linear cumulative count curves (McBreen et al. 2002). We argue that quiescent intervals seen in many GRB light curves arise due to inhomogeneities of the magnetic flux distribution inside the star. In at least one case, GRB 920513, there is a clear deviation from linear cumulative curve during the second half of that GRB. We infer the presence of a magnetised torus, or a “knot”, in the outer half of the star. In another case, GRB 940210, which shows two such deviations, we infer the pres-

ence of two such knots, with indications that the outermost knot contains a magnetic flux that exceeds the net flux through the star. While the magnetic field structure in the stellar interiors is an open question, knot-like magnetic flux configurations are expected from MHD stability arguments (Braithwaite & Spruit 2004; Braithwaite 2006). Statistical analysis of a larger number of GRB lightcurves might be a powerful probe of stellar magnetic structure.

## ACKNOWLEDGMENTS

We thank Eliot Quataert, Brian Metzger, and Omer Bromberg for valuable discussions. AT was supported by NASA through Einstein Postdoctoral Fellowship grant number PF3-140115 awarded by the Chandra X-ray Center, which is operated by the Smithsonian Astrophysical Observatory for NASA under contract NAS8-03060, and NASA via High-End Computing (HEC) Program through the NASA Advanced Supercomputing (NAS) Division at Ames Research Center that provided access to the Pleiades supercomputer, as well as NSF through an XSEDE computational time allocation TG-AST100040 on NICS Kraken, Nautilus, TACC Stampede, Maverick, and Ranch. DG acknowledges support from the Fermi 6 cycle grant number 61122. We used Enthought Canopy Python distribution to generate figures for this work.

## APPENDIX A: TIMESCALES INVOLVED IN CORE-COLLAPSE AND ACCRETION

As we discussed previously<sup>1</sup>, rotation in progenitor models is uncertain, and in fact it can exceed the Keplerian value (see Fig. 2b). Thus, in our work, we limit the rotation to be at most 10% of Keplerian value. The resulting angular momentum profile is shown in Fig. A1(a).

We assume that gas falls freely from its initial position  $r$ , until it hits the centrifugal barrier at the circularisation radius,  $r_D$ ,

$$\frac{r_D}{r} = \left( \frac{\ell}{\ell_K} \right)^2. \quad (\text{A1})$$

The ratio (A1) is shown in Fig. A1(b). Inside of  $r_D$ , gas travels viscously in the form of an accretion disk, with the accretion time

$$t_{\text{acc}} \approx \frac{r_D}{v_r} \approx \alpha^{-1} \left( \frac{R_{\text{circ}}}{r_g} \right)^{1/2} \left( \frac{h}{r} \right)^{-2} \frac{r_g}{c}. \quad (\text{A2})$$

Figure A1(c) shows the ratio if accretion time to free-fall time,  $t_{\text{ff}} = (2r_g/r)^{1/2}$ :

$$\frac{t_{\text{acc}}}{t_{\text{ff}}} = \frac{2^{1/2}}{\alpha} \left( \frac{r_D}{r} \right)^{3/2} \left( \frac{h}{r} \right)^{-2} = \frac{2^{1/2}}{\alpha} \left( \frac{\ell}{\ell_K} \right)^{3/2} \left( \frac{h}{r} \right)^{-2}. \quad (\text{A3})$$

In Fig. A1, for illustration we choose  $h/r = 1$  and  $\alpha = 0.1$ . Since gas transit time through the accretion disk is negligible compared to the free-fall time, we for simplicity ignore the accretion time. That said, there could be scenarios in which  $t_{\text{acc}} \gg t_{\text{ff}}$  (e.g., if stellar rotation is close to Keplerian). In such extreme cases, one does need to account for the accretion time.

## REFERENCES

- Birkel R., Aloy M. A., Janka H.-T., Müller E., 2007, *A&A*, 463, 51
- Bisnovatyi-Kogan G. S., Ruzmaikin A. A., 1974, *Ap&SS*, 28, 45
- Bisnovatyi-Kogan G. S., Ruzmaikin A. A., 1976, *Ap&SS*, 42, 401
- Blandford R. D., Begelman M. C., 1999, *MNRAS*, 303, L1

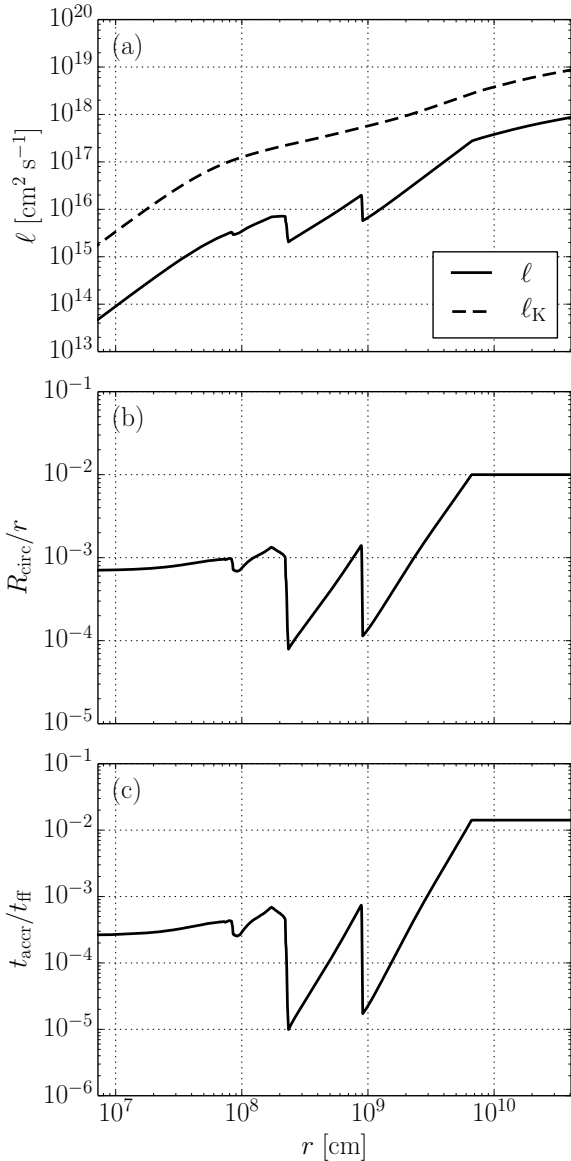


**Figure A1.** The rotation and time-scales in model 16TI. As we discussed previously<sup>1</sup>, rotation in progenitor models is uncertain, and in fact it can exceed the Keplerian value. Thus, in our work, we limit the rotation to be at most 10% of Keplerian value. The resulting angular momentum profile is shown in **Panel (a)** with the solid line; the Keplerian angular momentum is shown with the dashed line. We assume that gas falls freely from its initial position  $r$ , until it hits the centrifugal barrier at the circularisation radius,  $R_{\text{circ}}$ ; the ratio of the two is shown in **Panel (b)**. Inside of that radius, gas travels viscously in the form of an accretion disk, with the accretion time  $t_{\text{acc}} \approx r/v_r$ , that is much shorter than the free-fall time,  $t_{\text{ff}}$ , as seen in **Panel (c)**. In the plot, we set  $h/r = 1$  and  $\alpha = 0.1$ . Since gas transit time though the accretion disk is negligible compared to the free-fall time, we for simplicity ignore it.

Blandford R. D., Znajek R. L., 1977, MNRAS, 179, 433  
 Braithwaite J., 2006, A&A, 453, 687  
 Braithwaite J., Spruit H. C., 2004, Nature, 431, 819  
 Bromberg O., Granot J., Lyubarsky Y., Piran T., 2014, ArXiv:1402.4142  
 Bromberg O., Granot J., Piran T., 2014, ArXiv:1407.0123  
 Bromberg O., Nakar E., Piran T., Sari R., 2012, ApJ, 749, 110  
 Bromberg O., Nakar E., Piran T., Sari R., 2013, ApJ, 764, 179  
 Chen W.-X., Beloborodov A. M., 2007, ApJ, 657, 383

Galama T. J., et al., 1998, Nature, 395, 670  
 Guetta D., Piran T., Waxman E., 2005, ApJ, 619, 412  
 Igumenshchev I. V., Narayan R., Abramowicz M. A., 2003, ApJ, 592, 1042  
 Kawka A., Vennes S., Schmidt G. D., Wickramasinghe D. T., Koch R., 2007, ApJ, 654, 499  
 Komissarov S. S., Barkov M. V., 2009, MNRAS, 397, 1153  
 Kouveliotou C., et al., 1993, ApJ, 413, L101  
 Krolik J. H., Piran T., 2011, ApJ, 743, 134  
 Külebi B., Jordan S., Euchner F., Gänsicke B. T., Hirsch H., 2009, A&A, 506, 1341  
 Kumar P., Narayan R., 2009, MNRAS, 395, 472  
 Kumar P., Narayan R., Johnson J. L., 2008a, MNRAS, 388, 1729  
 Kumar P., Narayan R., Johnson J. L., 2008b, Science, 321, 376  
 Kumar P., Panaitescu A., 2000, ApJ, 541, L51  
 Leng M., Giannios D., 2014, ApJ, 445  
 Levan A. J., Tanvir N. R., Starling R. L. C., et al., 2014, ApJ, 781, 13  
 Levinson A., Begelman M. C., 2013, ApJ, 764, 148  
 Levinson A., Eichler D., 2003, ApJ, 594, L19  
 MacFadyen A. I., Woosley S. E., 1999, ApJ, 524, 262  
 McBreen S., McBreen B., Hanlon L., Quilligan F., 2002, A&A, 393, L29  
 McKinney J. C., Tchekhovskoy A., Blandford R. D., 2012, MNRAS, 423, 3083  
 Meszaros P., Rees M. J., 1997, ApJ, 482, L29  
 Metzger B. D., Giannios D., Thompson T. A., Bucciantini N., Quataert E., 2011, MNRAS, 413, 2031  
 Modjaz M., Kewley L., Kirshner R. P., Stanek K. Z., Challis P., Garnavich P. M., Greene J. E., Kelly P. L., Prieto J. L., 2008, AJ, 135, 1136  
 Modjaz M., Stanek K. Z., Garnavich P. M., Berlind P., Blondin S., Brown W., Calkins M., Challis P., Diamond-Stanic A. M., Hao H., Hicken M., Kirshner R. P., Prieto J. L., 2006, ApJ, 645, L21  
 Morsony B. J., Lazzati D., Begelman M. C., 2010, ApJ, 723, 267  
 Nakar E., Piran T., 2002, MNRAS, 331, 40  
 Narayan R., Igumenshchev I. V., Abramowicz M. A., 2003, PASJ, 55, L69  
 Narayan R., Kumar P., 2009, MNRAS, 394, L117  
 Narayan R., Paczynski B., Piran T., 1992, ApJ, 395, L83  
 Narayan R., Sądowski A., Penna R. F., Kulkarni A. K., 2012, MNRAS, 426, 3241  
 Nousek J. A., Kouveliotou C., Grupe D., et al., 2006, ApJ, 642, 389  
 Popham R., Woosley S. E., Fryer C., 1999, ApJ, 518, 356  
 Quilligan F., McBreen B., Hanlon L., McBreen S., Hurley K. J., Watson D., 2002, A&A, 385, 377  
 Ramirez-Ruiz E., Fenimore E. E., 2000, ApJ, 539, 712  
 Ruffert M., Janka H.-T., 1999, A&A, 344, 573  
 Sądowski A., Narayan R., Penna R., Zhu Y., 2013, MNRAS, 436, 3856  
 Sądowski A., Narayan R., Tchekhovskoy A., Abarca D., Zhu Y., McKinney J. C., 2014, ArXiv:1407.4421  
 Stanek K. Z., et al., 2003, ApJ, 591, L17  
 Tchekhovskoy A., McKinney J. C., Narayan R., 2012, Proceedings of the conference "The Central Kiloparsec in Galactic Nuclei: Astronomy at High Angular Resolution 2011", open access Journal of Physics: Conference Series (JPCS), published by IOP Publishing, arXiv:1202.2864  
 Tchekhovskoy A., Metzger B. D., Giannios D., Kelley L. Z., 2014, MNRAS, 437, 2744  
 Tchekhovskoy A., Narayan R., McKinney J. C., 2010, ApJ, 711, 50  
 Tchekhovskoy A., Narayan R., McKinney J. C., 2011, MNRAS, 418, L79  
 Usov V. V., 1992, Nature, 357, 472  
 Wanderman D., Piran T., 2010, MNRAS, 406, 1944  
 Woosley S. E., 1993, ApJ, 405, 273  
 Woosley S. E., Heger A., 2006, ApJ, 637, 914  
 Zalamea I., Beloborodov A. M., 2011, MNRAS, 410, 2302  
 Zhang W., Woosley S. E., MacFadyen A. I., 2006, Journal of Physics Conference Series, 46, 403